

115, 1627 (1959).

<sup>11</sup>W. W. Daehnick, Phys. Rev. **177**, 1763 (1969).

<sup>12</sup>R. Moyer, unpublished.

<sup>13</sup>R. H. Bassel, R. M. Drisko, and G. R. Satchler, Oak Ridge National Laboratory Report No. ORNL-3240, 1962 (unpublished).

<sup>14</sup>P. D. Kunz, University of Colorado, code DWUCK Version II, 1969 (unpublished).

<sup>15</sup>P. J. A. Buttle and L. J. B. Goldfarb, Proc. Phys. Soc. (London) **83**, 701 (1964).

<sup>16</sup>J. K. Dickens, R. M. Drisko, F. G. Perey, and G. R. Satchler, Phys. Lett. **15**, 337 (1965).

<sup>17</sup>T. S. Bhatia, W. W. Daehnick, and T. R. Canada, Phys. Rev. C **3**, 1361 (1971).

<sup>18</sup>J. E. Holden, J. J. Kolata, and W. W. Daehnick, Phys. Rev. C **6**, 1305 (1972).

<sup>19</sup>E. R. Flynn, D. D. Armstrong, and J. G. Beery, Phys.

Rev. **182**, 1113 (1969).

<sup>20</sup>R. H. Bassel, Phys. Rev. **149**, 791 (1966).

<sup>21</sup>B. F. Bayman and A. Kallio, Phys. Rev. **156**, 1121 (1967).

<sup>22</sup>R. DelVecchio and W. W. Daehnick, Phys. Rev. C **6**, 2095 (1972), and references therein.

<sup>23</sup>W. W. Daehnick and Y. S. Park, Phys. Rev. **180**, 1062 (1969).

<sup>24</sup>J. J. Kolata, W. W. Daehnick, and J. E. Holden, Phys. Rev. C **6**, 1312 (1972).

<sup>25</sup>Y. S. Park, Ph.D. thesis, Univ. of Pittsburgh, 1968 (unpublished).

<sup>26</sup>R. M. Drisko and F. Rybicki, Phys. Rev. Lett. **16**, 275 (1966).

<sup>27</sup>M. J. Schneider and W. W. Daehnick, Phys. Rev. C **4**, 1649 (1971).

<sup>28</sup>M. B. Lewis and W. W. Daehnick, Phys. Rev. C **1**, 1577 (1970).

PHYSICAL REVIEW C

VOLUME 7, NUMBER 6

JUNE 1973

## Properties of $\gamma$ -Ray Transitions in $^{56}\text{Co}$ from $^{56}\text{Ni}$ Decay and $^{56}\text{Fe}(p, n\gamma)^{56}\text{Co}$

L. E. Samuelson, W. H. Kelly, and R. R. Todd\*

*Cyclotron Laboratory,† Department of Physics, Michigan State University, East Lansing, Michigan 48823*

R. A. Warner, Wm. C. McHarris,‡ and F. M. Bernthal

*Department of Chemistry§ and Cyclotron Laboratory,† Department of Physics, Michigan State University, East Lansing, Michigan 48823*

E. M. Bernstein and R. Shamu

*Department of Physics,¶ Western Michigan University, Kalamazoo, Michigan 49001*

(Received 22 December 1972)

The  $^{56}\text{Ni}$   $\epsilon$  decay and the  $^{56}\text{Fe}(p, n\gamma)^{56}\text{Co}$  reaction with beam energies between 5.5 and 8.4 MeV have been used with Ge(Li) spectrometers to study the properties of  $\gamma$  rays from states of  $^{56}\text{Co}$  below 2.86 MeV excitation. From  $^{56}\text{Ni}$   $\epsilon$  decay both the  $\gamma$ -ray spectrum and  $\gamma$ - $\gamma$  coincidences were studied.  $\gamma$ - $\gamma$  coincidences,  $\gamma$ -ray excitation functions,  $\gamma$ -ray angular distributions, and absolute cross sections were measured for the  $^{56}\text{Fe}(p, n\gamma)^{56}\text{Co}$  reaction. An  $\epsilon$  decay scheme for  $^{56}\text{Ni}$ , which includes six  $\gamma$  rays, and an energy-level diagram for  $^{56}\text{Co}$ , which includes 35  $\gamma$  rays (14 of which are reported for the first time) from 20 excited states, are presented. Comparison of the data from  $^{56}\text{Fe}(p, n\gamma)^{56}\text{Co}$  with predictions of the statistical compound-nuclear model have resulted in spin assignments (in parentheses) for the following states (energies in keV) of  $^{56}\text{Co}$ : 158.4(3), 576.6(5), 829.7(4), 970.3(2), 1009.2(5), 1114.6(3), 1450.8(0), and 1720.3(1). Branching ratios are presented for 14  $\gamma$  rays from these eight states and multipole mixing ratios are given for 12 of these  $\gamma$  rays (10 are predominantly M1). The data are consistent with a spin-4 assignment to the ground state. Contrary to previous suggestions, evidence from all experiments indicates that only one state (believed to be the antianalog of the  $^{56}\text{Fe}$  ground state) exists in  $^{56}\text{Co}$  in the neighborhood of 1451 keV excitation. The level energies,  $\gamma$ -ray multipole mixing ratios, and  $\gamma$ -ray branching ratios agree, in general, with shell-model predictions of McGrory.

### I. INTRODUCTION

The earliest investigations<sup>1-4</sup> of the low-lying excited states of  $^{56}\text{Co}$  began with the  $\epsilon$  decay of  $^{56}\text{Ni}$ . These studies, which included measurements of the  $^{56}\text{Ni}$  half-life,<sup>1</sup> the  $\gamma$ -ray spectrum,<sup>1,3,4</sup>  $\gamma$ - $\gamma$  angular correlations,<sup>1,3</sup> the internal-conversion electron spectrum,<sup>2</sup> and lifetimes of some

$^{56}\text{Co}$  states,<sup>1</sup> produced valuable information. However, only selected states below 2.1 MeV could be populated and unambiguous spin assignments for these states could not be made.

More recently, experiments involving the two-particle transfer reactions,  $^{54}\text{Fe}(^3\text{He}, p)^{56}\text{Co}$ ,<sup>5-9</sup>  $^{54}\text{Fe}(\alpha, d)^{56}\text{Co}$ ,<sup>10</sup>  $^{58}\text{Ni}(p, ^3\text{He})^{56}\text{Co}$ ,<sup>11</sup> and  $^{58}\text{Ni}(d, \alpha)^{56}\text{Co}$ ,<sup>6,7,9,12,13</sup> and the charge-exchange reactions,

$^{56}\text{Fe}(p,n)^{56}\text{Co}$ <sup>14,15</sup> and  $^{56}\text{Fe}(^3\text{He},t)^{56}\text{Co}$ <sup>16-19</sup> have increased the knowledge of the properties of these and additional states. However, the interpretations of these experiments depend strongly upon assumed  $^{56}\text{Co}$  wave functions and reaction mechanisms. Neither is well known.

In particular, the  $J^\pi$  of a state in  $^{56}\text{Co}$  at 1451 keV has been somewhat controversial. In the early  $^{56}\text{Ni}$  decay work,  $1^-$  or  $2^+$  seemed most consistent with the data, with  $1^-(2^-)$  being favored by Ohnuma *et al.*<sup>3</sup> and  $2^+$  by Jenkins and Meyerhof<sup>2</sup> and Wells.<sup>20</sup> Later, Belote, Dorenbusch, and Rapaport<sup>6</sup> observing  $l=0$  transfers in  $(^3\text{He},p)$  and  $(d,\alpha)$  reactions and a weak  $(d,\alpha)$  cross section chose  $0^+$ . Belote *et al.*<sup>6</sup> then conjectured that this state was an antianalog of the  $^{56}\text{Fe}$  ground state ( $J^\pi=0^+$ ). Subsequent particle transfer work has confirmed  $J^\pi=0^+$  (e.g., see Refs. 9 and 11). However, Roos and Goodman<sup>17</sup> reported an  $l=1$  transfer in the  $(^3\text{He},t)$  reaction, implying  $J^\pi=1^-$ ; they then suggested that possibly a  $0^+$  and a  $1^-$  state occur within a few keV of each other at this energy.

The  $^{56}\text{Fe}(p,n\gamma)^{56}\text{Co}$  reaction<sup>21,22</sup> near threshold was chosen for the present study because the reaction should be well described by the statistical compound nuclear (CN) theories of Wolfenstein,<sup>23</sup> Hauser and Feshbach,<sup>24</sup> Biedenharn and Rose,<sup>25</sup> Satchler,<sup>26</sup> and Sheldon and Van Patter.<sup>27</sup> Since all states for which the incoming energy and angular momentum are sufficient should be excited in this type of reaction, both members of the doublet (if they exist) at 1451 keV should be populated quite strongly because of their expected low spins. Comparisons of the results of the present work with the predictions of the statistical CN theory and with previously measured  $^{56}\text{Co}$   $\gamma$ -ray characteristics have led to unambiguous spin assignments for all  $^{56}\text{Co}$  states below 1.8 MeV. In addition,  $\gamma$ -ray multipole mixing ratios, precise level energies, and  $\gamma$ -ray branching ratios are obtained. This experimental information is compared with shell-model

level energies and  $B(M1)$  and  $B(E2)$  values for  $^{56}\text{Co}$  calculated recently by McGrory.<sup>28</sup>

As a supplement to the  $(p,n\gamma)$  work, the  $\gamma$ -ray spectrum accompanying the  $^{56}\text{Ni}$   $\epsilon$  decay was re-investigated. These experiments corroborated the previous  $^{56}\text{Ni}$  decay work and the energies of some  $\gamma$  rays in  $^{56}\text{Co}$ . In particular, the 1451-keV state was examined very carefully in the  $\epsilon$ -decay study for any evidence of its being a doublet.

## II. $\epsilon$ DECAY OF $^{56}\text{Ni}$

Ge(Li) detectors were used to measure the  $\gamma$ -ray spectrum and  $\gamma$ - $\gamma$  coincidences accompanying the  $^{56}\text{Ni}$   $\epsilon$  decay. These experiments yielded  $\gamma$ -ray energies and intensities and confirmed the placement of  $\gamma$  rays in the  $^{56}\text{Ni}$  decay scheme.

### A. Source Preparation

The 6.1-day  $^{56}\text{Ni}$  activities were produced via the  $^{56}\text{Fe}(^3\text{He},3n)^{56}\text{Ni}$  reaction ( $Q=-16.3$  MeV) by bombarding 0.02-g/cm<sup>2</sup> iron foils with 45-MeV  $^3\text{He}$  particles from the Michigan State University (MSU) sector-focussed cyclotron. After allowing about 10 days for the undesired 1.5-day  $^{57}\text{Ni}$  activity to decay, chemical separations were performed.

The iron foils were first dissolved in hot 15 *N* HCl, evaporated to dryness, and redissolved in 10 *N* HCl. The samples were then passed through a column of Dowex 1-X8 anion exchange resin previously brought into equilibrium with 10 *N* HCl. This procedure<sup>29</sup> removed all detectable contaminant cobalt activities such as  $^{56}\text{Co}$  and  $^{58}\text{Co}$ . The desired  $^{56}\text{Ni}$  activities were then separated from the remaining contaminant radioisotopes such as  $^{51}\text{Cr}$ ,  $^{52}\text{Mn}$ , and  $^{54}\text{Mn}$  by the standard procedure of precipitation of nickel dimethylglyoxime (Ni-DMG).<sup>30</sup> The Ni-DMG was finally dissolved in 15 *N* HCl and placed in thin-walled plastic vials for counting.

### B. $\gamma$ -Ray Spectrum

Three different Ge(Li) detectors were used to take  $\gamma$ -ray singles spectra: (1) a 2.5%-efficient [compared to a 7.6-cm  $\times$  7.6-cm NaI(Tl) detector at 25 cm and at a  $\gamma$ -ray energy of 1332 keV] Ge(Li) detector with a 15:1 peak-to-Compton ratio and a full width at half maximum (FWHM) resolution of 2.34 keV at a  $\gamma$ -ray energy of 1332 keV; (2) a 4.5%-efficient Ge(Li) detector with a 22:1 peak-to-Compton ratio and a FWHM resolution of 2.10 keV; and (3) a 10.4%-efficient Ge(Li) detector with a 30:1 peak-to-Compton ratio and a FWHM resolution of 2.28 keV. A  $^{56}\text{Ni}$  decay  $\gamma$ -ray singles spectrum is shown in Fig. 1. Optimum resolution and the most symmetric peaks were obtained using an

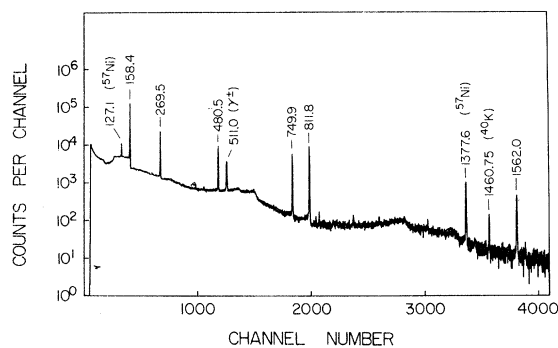


FIG. 1.  $^{56}\text{Ni}$  singles  $\gamma$ -ray spectrum taken with the 2.5%-efficient Ge(Li) spectrometer.

ORTEC model No. 450 research amplifier direct-coupled into a Northern Scientific 50-MHz analog-to-digital converter (ADC). The data were accumulated in either the MSU Cyclotron Laboratory's Xerox Data System  $\Sigma$ -7 time-sharing computer using a pulse-height analysis routine,<sup>31</sup> or in a Digital Equipment Corporation PDP-9 computer loaded with another pulse-height analysis routine. Peak centroids and areas were determined off line by the peak-fitting code SAMPO,<sup>32</sup> which was especially useful in stripping unresolved multiplets.

Since it offered the best over-all resolution, the 4.5%-efficient Ge(Li) detector was used to take the spectra for the  $\gamma$ -ray energy measurements. For these measurements, spectra from a  $^{56}\text{Ni}$  source were taken in the presence of various combinations of such well-known  $\gamma$ -ray energy standards<sup>33,34</sup> as  $^{57}\text{Co}$ ,  $^{139}\text{Ce}$ ,  $^{203}\text{Hg}$ ,  $^{51}\text{Cr}$ ,  $^{207}\text{Bi}$ ,  $^{137}\text{Cs}$ ,  $^{54}\text{Mn}$ ,  $^{56}\text{Co}$ ,  $^{88}\text{Y}$ ,  $^{65}\text{Zn}$ ,  $^{60}\text{Co}$ ,  $^{22}\text{Na}$ ,  $^{40}\text{K}$ , and  $^{192}\text{Ir}$ . Care was taken so that standard peaks and the  $^{56}\text{Ni}$  decay peaks grew into the spectra at roughly equal rates. Quadratic fits were then made to the calibration energies versus measured centroids in two energy regions (100–800 keV and 700–2000 keV). The  $^{56}\text{Co}$   $\gamma$ -ray energies were then calculated by computer using these calibrations and are listed in Table I.

The 2.5%- and 10.4%-efficient Ge(Li) detectors were both used for the  $\gamma$ -ray intensity determinations. The relative  $\gamma$ -ray efficiency curves for both detectors were determined using the  $\gamma$ -ray intensity standards,  $^{160}\text{Tb}$ ,  $^{203}\text{Hg}$ ,  $^{180\text{m}}\text{Hf}$ ,  $^{110\text{m}}\text{Ag}$ ,  $^{177\text{m}}\text{Lu}$ ,  $^{56}\text{Co}$ ,  $^{88}\text{Y}$ ,  $^{60}\text{Co}$ , and  $^{24}\text{Na}$ . The relative intensities of the  $\gamma$  rays from these standards can be found elsewhere.<sup>35–38</sup> Separate singles spectra were taken using each detector with the  $^{56}\text{Ni}$  source placed both at 5 cm and at 25 cm from the face of the detector. The intensities presented in Table I were then obtained by averaging these four sets of data. The use of two detectors with highly differ-

ent efficiencies and of two source-to-detector distances allowed for sum-peak identification. Background spectra were also taken with each detector.

### C. $\gamma$ - $\gamma$ Coincidence

Prompt  $\gamma$ -ray coincidences in the  $^{56}\text{Ni}$   $\gamma$  decay were determined with a Ge(Li)-Ge(Li) spectrometer using the 4.5%- and 10.4%-efficient detectors arranged in  $150^\circ$  geometry with a graded (Pb-Sn-Cu) absorber placed between them to minimize Compton scattering from one detector into the other. A typical two-parameter, fast-slow coincidence arrangement (resolving time  $2\tau \approx 100$  nsec) was used. Addresses corresponding to the energies of coincident  $\gamma$  rays were listed in pairs on magnetic tape.<sup>39</sup> This listing yielded a  $4096 \times 4096$ -channel array of prompt coincidence events which were later sorted off line in gated slices.<sup>40</sup> The gated slices included careful subtraction of background coincidences which were determined from the adjacent continuum.

The integral coincidence spectrum from each detector is shown at the top of Fig. 2. The  $x$  axis was taken with the 4.5%-efficient detector, while the  $y$  axis was taken with the 10.4%-efficient detector. Each spectrum represents 330 000 coincidences. Beneath each integral spectrum in Fig. 2 are shown spectra in coincidence with the various  $^{56}\text{Co}$  peaks of the opposite axis. The results are summarized in Table II.

### D. $^{56}\text{Ni}$ $\epsilon$ -Decay Scheme

The  $^{56}\text{Ni}$   $\epsilon$ -decay scheme is shown in Fig. 3. Corrections for internal conversion are included using conversion coefficients measured by Jenkins and Meyerhof.<sup>2</sup> The intensities are normalized to 100 for the 158.4-keV transition strength. The values shown for the half-life of  $^{56}\text{Ni}$  and the half-lives of the 158.4-, 970.2-, and 1450.7-keV states of  $^{56}\text{Co}$  are those measured by Wells, Blatt, and Meyerhof.<sup>1</sup> The  $Q_\epsilon$  value of  $2.134 \pm 0.011$  MeV is from mass differences recently calculated by Ewbank

TABLE I. Energies and relative intensities of the  $\gamma$  rays in  $^{56}\text{Co}$  from the  $^{56}\text{Ni}$   $\epsilon$ - $^{56}\text{Co}$  decay.

$E_\gamma$ (keV)		$I_\gamma$	
Present work	Piluso <i>et al.</i> <sup>a</sup>	Present work	Piluso <i>et al.</i> <sup>b</sup>
$158.4 \pm 0.1$	$158.3 \pm 0.2$	$\equiv 100$	$\equiv 100$
$269.5 \pm 0.1$	$269.6 \pm 0.1$	$36.0 \pm 1.4$	$40.0 \pm 0.7$
$480.5 \pm 0.1$	$480.7 \pm 0.1$	$36.0 \pm 1.5$	$41.4 \pm 1.4$
$749.9 \pm 0.1$	$750.6 \pm 0.1$	$50.5 \pm 2.5$	$54.3 \pm 3.5$
$811.8 \pm 0.1$	$812.2 \pm 0.2$	$88.5 \pm 4.4$	$91.3 \pm 3.5$
$1562.0 \pm 0.2$	$1562.5 \pm 0.2$	$14.3 \pm 1.4$	$12.8 \pm 1.4$

<sup>a</sup> See Ref. 4.

<sup>b</sup> The relative  $\gamma$ -ray intensities presented by Piluso *et al.* (Ref. 4) have been renormalized here to 100 for the intensity of the 158.4-keV transition.

TABLE II. Summary of two-parameter  $\gamma$ - $\gamma$  coincidence results for the  $^{56}\text{Ni}$   $\epsilon$ - $^{56}\text{Co}$  decay.

$E_\gamma/E_\gamma$ (keV)	158	270	481	511( $\gamma^\pm$ )	750	812	1562
158	...	Yes	Yes	No	Yes	Yes	Yes
270	Yes	...	Yes	No	No	Yes	No
481	Yes	Yes	...	No	No	Yes	No
511( $\gamma^\pm$ )	No	No	No	...	No	No	No
750	Yes	No	No	No	...	Yes	No
812	Yes	Yes	Yes	No	Yes	...	No
1562	Yes	No	No	No	No	No	...

and Raman.<sup>41</sup> The spin and parity assignments shown are based on  $^{56}\text{Fe}(p, n\gamma)^{56}\text{Co}$  experiments and will be discussed in detail later.

The limits on the  $\epsilon$ -feeding intensities and associated  $\log ft$  values shown in Fig. 3 were computed using the experimental uncertainties in the imbalances of the electromagnetic decay intensities. A minimum of 96% and a maximum of 100% for  $\epsilon$  feeding to the 1720.2-keV state result in a  $\log ft$

between 4.38 and 4.40. The 4.39 value shown in Fig. 3 is an average of these two values. A recent shell-model calculation by Goode and Zamick<sup>42</sup> predicts  $\log ft = 5.8$  for this  $0^+$  to  $1^+$  allowed transition. Although the  $\log ft$  value 4.39 measured here is much smaller than the value 5.8 predicted, it is still considerably larger than the value 2.5 predicted using simple shell-model wave functions.<sup>42</sup> Goode and Zamick's explanation that this decay

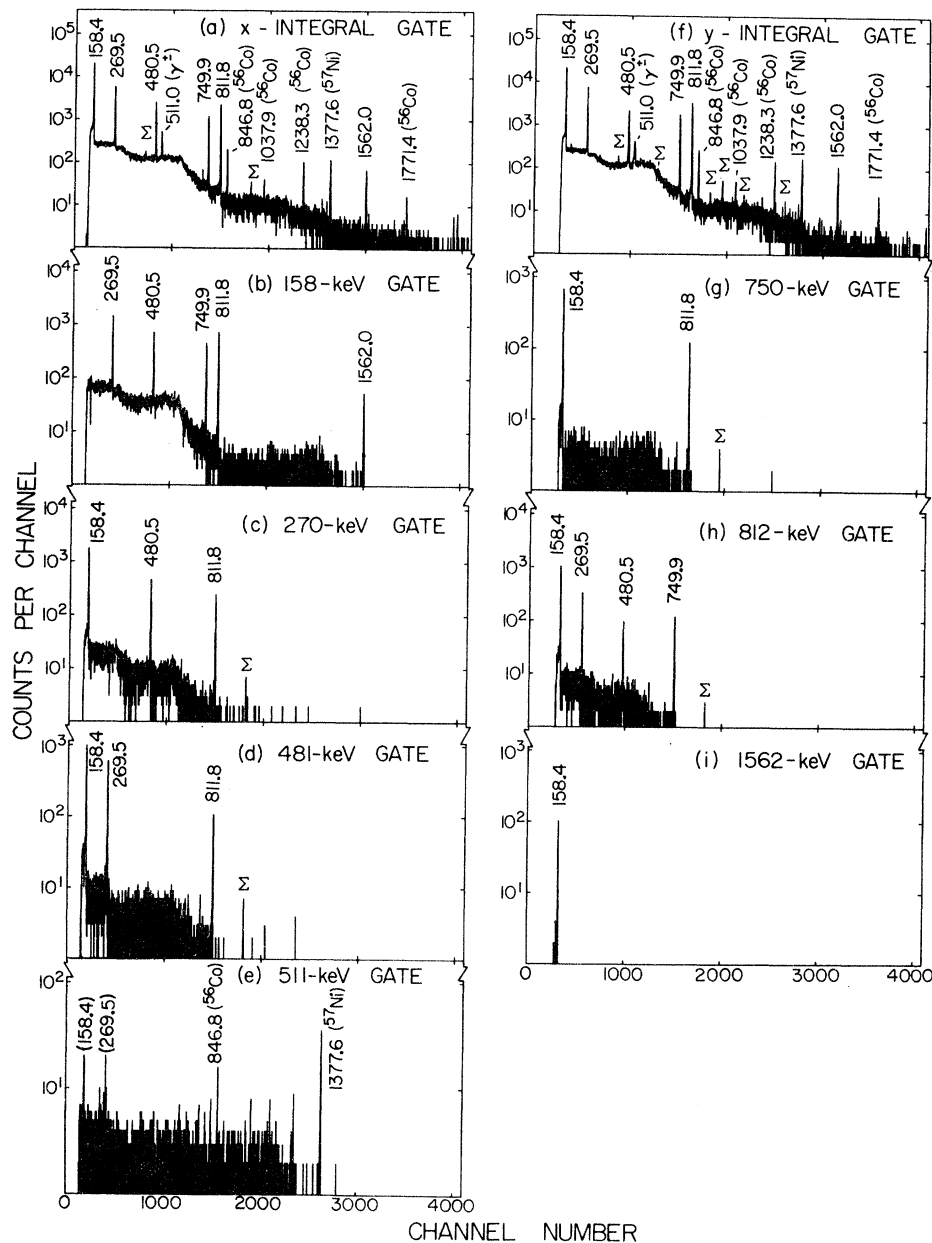


FIG. 2. Integral coincidence and gated spectra from the  $^{56}\text{Ni}$   $\gamma$ - $\gamma$  coincidence experiment. Peaks labeled with a  $\Sigma$  were identified as triple coincidences where two of the three coincident  $\gamma$  rays have been summed in one detector. Peaks labeled in parentheses are believed to be from chance coincidences or insufficient background subtraction.

goes almost entirely to the giant spin-isospin part of this  $1^+$  state in  $^{56}\text{Co}$  and is hindered because this part is small, is probably correct. However, their estimate of the magnitude of this portion of the wave function must be too small as indicated by the difference between the predicted and measured  $\log ft$  values.

A maximum of 2%  $\epsilon$  feeding to the 1450.7-keV state yields  $\log ft > 6.5$ . The  $0^+$  to  $0^+$  transition to this state is an isospin-forbidden ( $\Delta T = 1$ ) Fermi transition<sup>43</sup> for which one might expect<sup>44</sup>  $\log ft \approx 7.8$ . Assuming isospin forbiddenness to be a weak rule, the apparent hindrance of  $\epsilon$  decay to this state can be explained in simple terms by the fact that the  $0p$ - $0h$  component of the  $^{56}\text{Ni}$  ground state cannot decay readily to  $2p$ - $2h$  components of states in  $^{56}\text{Co}$ . The 1450.7-keV state must be predominantly  $2p$ - $2h$  however, since no low-lying states in  $^{56}\text{Co}$  can have  $1p$ - $1h$  coupled to  $J^\pi = 0^+$ . Thus, any  $\epsilon$  decay between these states must involve  $2p$ - $2h$  components of the  $^{56}\text{Ni}$  ground state. Goode and Zamick<sup>42</sup> estimate the amount of  $2p$ - $2h$  admixture in the  $^{56}\text{Ni}$  ground state at 26%. Since there must still be many  $2p$ - $2h$  components in this admixture which do not overlap with those of the 1450.7-keV

$^{56}\text{Co}$  state, the  $\epsilon$  transition between these two states would thus be expected to be considerably hindered.

The lower limits of 6.4 and 7.7 on the  $\log ft$  values for the  $0^+$  to  $2^+$  transition to the 970.2-keV state and the  $0^+$  to  $3^+$  transition to the 158.4-keV state, respectively, are very small compared to  $\log ft \approx 12$  expected<sup>44</sup> for these second-forbidden transitions. These limits reflect errors in small differences between large numbers.

The  $Q_\epsilon$  value of 2.134 MeV allows the possibility of positron decay to the ground state and the 158.4- and 970.2-keV states. The  $\epsilon(K)/\beta^+$  ratios for  $\beta$  transitions to these states are estimated<sup>35</sup> to be 0.31, 0.52, and 540, respectively. Any decay strength to the 970.2-keV state is thus expected to be mostly electron capture; however, considerable  $\beta^+$  emission would be expected to accompany any  $\beta$  decay to the ground and 158.4-keV states. The fact that no coincidences with the 511.0-keV annihilation radiation (other than chance) were observed in the  $^{56}\text{Ni}$  decay (see Fig. 2), supports the lack of  $\beta$  feeding to the 158.4-keV state as determined from  $\gamma$ -ray intensity imbalances and indicates that such  $\beta$  decay is forbidden. The upper limit of 0.01 per decay for the relative intensity of positron emission reported by Sheline and Stoughton<sup>45</sup> further supports this observation and also indicates little  $\beta$  feeding to the ground state as would be expected by the forbiddenness of this  $0^+$  to  $4^+$  transition.

Weak peaks seen at 427.9, 908.3, and 970.2 keV in the singles spectra taken with the  $^{56}\text{Ni}$  sources at 5 cm and weak peaks seen at 428, 639, 908, 970, 1081, and 1292 keV in the  $\gamma$ - $\gamma$  coincidence spectra were concluded to be sum-coincidence peaks, since they were only found to be in coincidence with appropriate members of the same  $\gamma$ -ray cascade and they all disappeared in singles spectra taken with the sources at 25 cm. (Observable intensities would have been expected if the peaks had been real.) Unfortunately, because of the longer counting time required, the possible 970.2-keV ground-state transition was masked somewhat in the 25-cm measurements by a 968.9-keV background  $\gamma$  radiation from the negatron decay of  $^{228}\text{Ac}$  (in the  $^{232}\text{Th}$   $\alpha$ -decay chain). However, the 970.2-keV peak apparently disappeared at the larger distance, since the centroid shifted between the 5-cm and the 25-cm measurements by the entire 1.3-keV difference between these two  $\gamma$  rays, and since the peak area at 25 cm was completely accounted for by taking the ratio (measured in the background spectrum) of the areas of the 968.9-keV peak and the slightly more intense 911.1-keV peak which branch from the same excited state in the  $^{228}\text{Th}$  daughter.<sup>35, 46</sup> There was no evidence to

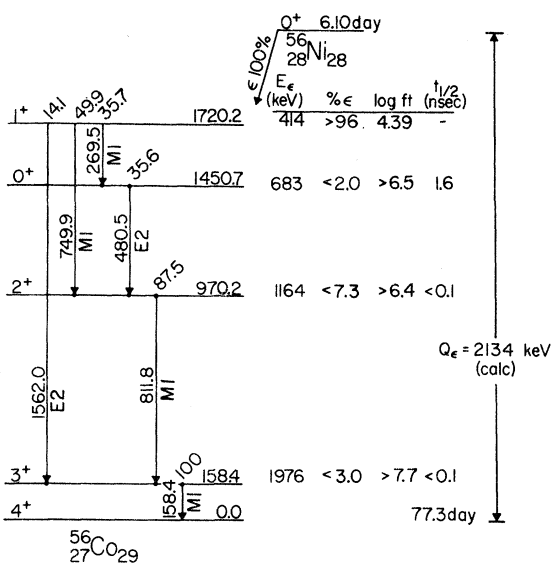


FIG. 3. Decay scheme of  $^{56}\text{Ni}$ . The  $\gamma$ -ray energies were measured using the  $^{56}\text{Ni}$  decay. The intensities are normalized to 100 for the 158.4-keV transition strength. The  $^{56}\text{Ni}$  decay half-life and the half-lives of the 158.4-, 970.2-, and 1450.7-keV states are from Ref. 1. The  $^{56}\text{Co}$  ground-state half-life is from Ref. 35. The  $Q_\epsilon$  value is from Ref. 41. The  $E_\epsilon$  values were calculated from the  $Q_\epsilon$  value and the measured level energies. The spin and parity assignments and  $\gamma$ -ray multiplicities (only the dominant multiplicities are shown) are from  $^{56}\text{Fe}(p,n\gamma)^{56}\text{Co}$  experiments and are discussed in Secs. III and IV.  $\log ft$  values are discussed in Sec. II D.

suggest changing the upper limits of 0.01 out of 100  $^{56}\text{Ni}$  decays reported by Piluso, Wells, and McDaniels<sup>4</sup> for the intensities of possible 970.2-, 1292.3-, 1450.7-, and 1720.2-keV  $\gamma$  rays.

A discussion of the 1451-keV excitation region is given in Sec. IV H.

### III. $^{56}\text{Fe}(p, n\gamma)^{56}\text{Co}$ REACTION

Four types of experiments were performed using the  $^{56}\text{Fe}(p, n\gamma)^{56}\text{Co}$  reaction ( $Q = -5.357$  MeV).<sup>47</sup> In the first type,  $\gamma$ - $\gamma$  coincidences were measured with a Ge(Li)-Ge(Li) spectrometer for  $^{56}\text{Co}$  excitations up to 2.86 MeV. These coincidences identified  $^{56}\text{Co}$   $\gamma$  rays and allowed placement in the excited-state level scheme. Except for the special cases of ground-state transitions with no coincidences, this method was very powerful. In the second type of experiment, excitation functions of the various  $^{56}\text{Co}$   $\gamma$  rays were measured from below the  $(p, n)$  threshold up to 2.26 MeV of excitation. Individual spectra provided  $\gamma$ -ray branching ratios, while the excitation functions provided threshold information (and, hence, evidence for  $\gamma$ -ray placement in the excited-state level scheme), information on relative cross sections as a function of proton energy (and, hence, evidence for spin assignments), and an indication of the level density and the degree of statistical averaging in the compound nucleus. In the third type of experiment, angular distributions of the various  $^{56}\text{Co}$   $\gamma$  rays were measured for excitations up to 1.91 MeV. Beam energies were chosen, where possible, such that the state in question was not fed from above by  $\gamma$ -ray transitions. The  $\gamma$ -ray angular distributions provided information on spins,  $\gamma$ -ray multipole mixing ratios, and  $\gamma$ -ray branching ratios. In the fourth type of experiment, absolute cross sections for excitations of the first eight excited states of  $^{56}\text{Co}$  were measured at a beam energy of 7.30 MeV. The experimental absolute cross sections offer direct comparisons with theoretical cross-section predictions of the statistical CN theory. In the following discussions,  $^{56}\text{Co}$   $\gamma$  rays and excited states are referred to with energies measured using the  $^{56}\text{Fe}(p, n\gamma)^{56}\text{Co}$  reaction. In a few instances these energies are slightly different from  $^{56}\text{Ni}$  decay values. The adopted energies appear in Sec. VI.

#### A. $\gamma$ - $\gamma$ Coincidences

Proton beams (all beam energies quoted in this paper are in the laboratory system) of 7.38 and 8.36 MeV (corresponding to excitations in  $^{56}\text{Co}$  of about 1.89 and 2.86 MeV, respectively) were obtained from the MSU cyclotron for the in-beam  $\gamma$ - $\gamma$  coincidence measurements. The target, obtained from the Isotope Division of Oak Ridge Na-

tional Laboratory, was a 0.90-mg/cm<sup>2</sup> iron foil enriched to 99.4%  $^{56}\text{Fe}$ . The 2.5%-efficient Ge(Li) detector (previously described) and a 7.4%-efficient Ge(Li) detector with a peak-to-Compton ratio of 25:1 and FWHM resolution of 3.5 keV were positioned as shown in Fig. 4. The lead block between the detectors has a 1.3-cm-diam hole drilled almost through it and served as a shielded beam stop as well as an attenuator for photons Compton scattered from one detector toward the other.

A typical two-parameter, fast-slow coincidence arrangement with constant-fraction timing discrimination was used. The single-channel analyzer window ( $2\tau \approx 50$  nsec) set on the output from a time-to-amplitude converter was a few nanoseconds less than the interval between cyclotron beam bursts. The 77-day half-life of the  $^{56}\text{Co}$  ground state resulted in minimal radioactivity buildup in the target and insured that most detected  $\gamma$  rays were from beam induced reactions. The coincidence events were stored on magnetic tape and later sorted off-line using background subtraction as described previously for the  $\epsilon$ -decay work. The 7.38-MeV spectra contained about one million coincidence events accumulated in 12 h of counting, while the 8.36-MeV spectra contained close to seven million coincidence events accumulated in 31 h. Typical singles counting rates for both experiments were 7000 cps in the 2.5%-efficient detector and 20 000 cps in the 7.4%-efficient detector. The average beam current was about 7 nA.

As a supplement to the coincidence experiments, the energies of those  $\gamma$  rays from the excited states of  $^{56}\text{Co}$  up to and including the 1720.3-keV state (excluding the 1561.7-keV  $\gamma$ ) were determined by

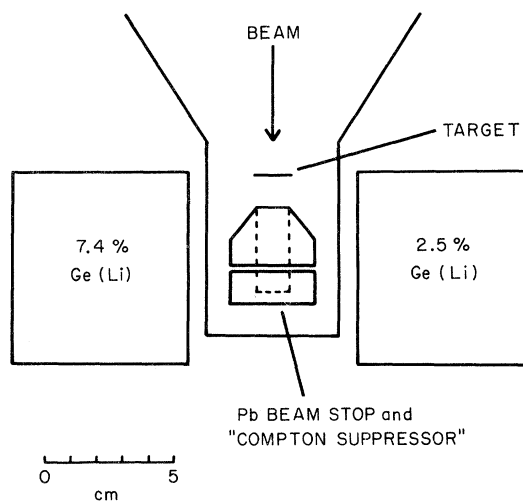


FIG. 4. Geometry for the in-beam  $\gamma$ - $\gamma$  coincidence measurements. The squares are not meant to represent the actual size of the Ge(Li) detectors, but only the approximate location of their cryostat caps.

taking a  $\gamma$ -ray singles spectrum of the  $^{56}\text{Fe}(p, n\gamma)$ - $^{56}\text{Co}$  reaction at  $E_p = 7.30$  MeV in the presence of such well-known  $\gamma$ -ray energy standards<sup>33,34</sup> as  $^{22}\text{Na}$ ,  $^{75}\text{Se}$ ,  $^{88}\text{Y}$ ,  $^{113}\text{Sn}$ , and  $^{137}\text{Cs}$ . The remaining energies of the 1561.7-keV  $\gamma$  and the  $\gamma$  rays from

TABLE III. Energies of  $\gamma$  rays found in  $^{56}\text{Co}$  at excitations up to 2.86 MeV from the  $^{56}\text{Fe}(p, n\gamma)^{56}\text{Co}$  reaction. Unless otherwise indicated, the identification of  $^{56}\text{Co}$   $\gamma$  rays is based upon both  $\gamma$ -ray excitation functions and  $\gamma$ - $\gamma$  coincidences.

Transition energies (keV)	
Present work <sup>a</sup>	$n$ - $\gamma$ coincidence (Ref. 22) <sup>b</sup>
158.4 ± 0.1	158.5
269.5 ± 0.1	269.7
285.0 ± 0.1	284.7
(424.7 ± 0.2) <sup>c</sup>	
432.8 ± 0.2	
480.5 ± 0.1	480.4
576.6 ± 0.1	576.4
671.3 ± 0.1	671.3
750.1 ± 0.1	750.0
811.9 ± 0.1	812.0
829.8 ± 0.1	830.0
945.5 ± 0.2	945.4
956.1 ± 0.3	
960.1 ± 0.2	959.6
1009.2 ± 0.1 <sup>d</sup>	1009.3
(1046.6 ± 0.5) <sup>c</sup>	
1090.1 ± 0.4 <sup>c</sup>	
1101.1 ± 0.5 <sup>c</sup>	
1110.0 ± 0.2	
1114.6 ± 0.1	1114.6
1184.9 ± 0.2 <sup>c</sup>	1184.6
1254.4 ± 0.3 <sup>c</sup>	
1319.8 ± 0.3 <sup>c</sup>	1317.9
1334.7 ± 0.3 <sup>c</sup>	
1387.3 ± 0.3 <sup>c</sup>	1387.1
(1459.1 ± 0.6) <sup>c</sup>	
1561.7 ± 0.4	
(1641.1 ± 0.7) <sup>c</sup>	
1760.1 ± 0.5 <sup>c</sup>	
1772.1 ± 0.4 <sup>c</sup>	1771.5
(1782.4 ± 0.6) <sup>c</sup>	
1892.7 ± 0.4 <sup>c</sup>	
1901.5 ± 0.4	1901.3
2066.1 ± 0.4 <sup>c</sup>	2066.5
2131.1 ± 0.5 <sup>c</sup>	2129.5
2146.4 ± 0.5 <sup>c</sup>	2145.0
2198.7 ± 0.5 <sup>c</sup>	
(2313.3 ± 0.9) <sup>c</sup>	
2451.1 ± 0.7 <sup>c</sup>	
2488.8 ± 0.7 <sup>c</sup>	
2506.7 ± 0.7 <sup>c</sup>	

<sup>a</sup> Those  $\gamma$ -ray energies presented in parentheses are from weak transitions believed to belong to  $^{56}\text{Co}$  but which could not be placed in the decay scheme.

<sup>b</sup> The energy errors of all  $\gamma$  rays listed are  $\pm 0.5$  keV.

<sup>c</sup> Identification was based upon  $\gamma$ - $\gamma$  coincidences only.

<sup>d</sup> Identification was based upon  $\gamma$ -ray excitation functions only.

the excited states of 1930.4 keV and above were determined from the various  $\gamma$ - $\gamma$  coincidence gated spectra. In both cases, prominent  $^{56}\text{Fe}$   $\gamma$  rays from the  $^{56}\text{Fe}(p, p'\gamma)$  reaction were used as some of the energy standards.<sup>38,48</sup> For the  $\gamma$ -ray energy determinations from the  $\gamma$ -ray singles data, a quadratic fit was made to the measured centroids (analyzed by SAMPO<sup>32</sup>) versus calibration energies in one energy region (120–1300 keV). For the  $\gamma$ -ray energy determinations from the  $\gamma$ - $\gamma$  coincidence data, a similar quadratic fit was made in one energy region (800–3000 keV). In the latter, the  $^{56}\text{Fe}$  calibration peak centroids were determined from a spectrum gated on the intense  $^{56}\text{Fe}$  846.8-keV  $\gamma$  peak. The  $^{56}\text{Co}$   $\gamma$ -ray energies were then calculated by computer using the appropriate calibration curve. The energies of the six  $\gamma$  rays found in both the  $^{56}\text{Ni}$  decay and the  $^{56}\text{Fe}(p, n\gamma)^{56}\text{Co}$  reaction agree to within the experimental errors (see Tables I and III). The adopted energies of these six  $\gamma$  rays are listed in Sec. VI.

The two integral spectra and some representative gated spectra from the coincidence experiment with  $E_p = 8.36$  MeV are shown in Fig. 5. 35  $\gamma$  rays were definitely identified to be from  $^{56}\text{Co}$ , and 6 others are possibly from the same nucleus. These include 21  $\gamma$  rays previously reported by DelVecchio, Gibson, and Daehnick<sup>22</sup> to be in coincidence with neutrons from the same reaction. The energies (as determined above) of the  $^{56}\text{Co}$   $\gamma$  rays are listed in Table III; the coincidence relationships between these  $\gamma$  rays are listed in Table IV. (For brevity, the coincidence data taken at  $E_p = 7.38$  MeV and many gated spectra taken at  $E_p = 8.36$  MeV are not shown here. All the gated coincidence spectra from which the coincidence relationships were derived and from which energy calibrations were determined can be found in an Appendix to Ref. 49.)

The excited-state level scheme in Fig. 6 is consistent with the coincidence data and the excitation function data (next section). Dots denote observed coincidence relationships between  $\gamma$ -ray transitions entering and leaving a state. The beam energies (and the corresponding maximum possible  $^{56}\text{Co}$  excitations) at which the coincidence and angular distribution data were taken are shown on the right. The spin assignments for states up to and including the 1720.3-keV state are based on the present experiments and will be discussed in detail later in Sec. IV. The spin and parity assignments to the states at 1930.4 keV and above are those of Schneider and Daehnick<sup>9</sup> and are consistent with these and other experiments.

The positive parities shown in Fig. 6, up to and including that for the 1720.3-keV state, could not be determined in the present work and are there-

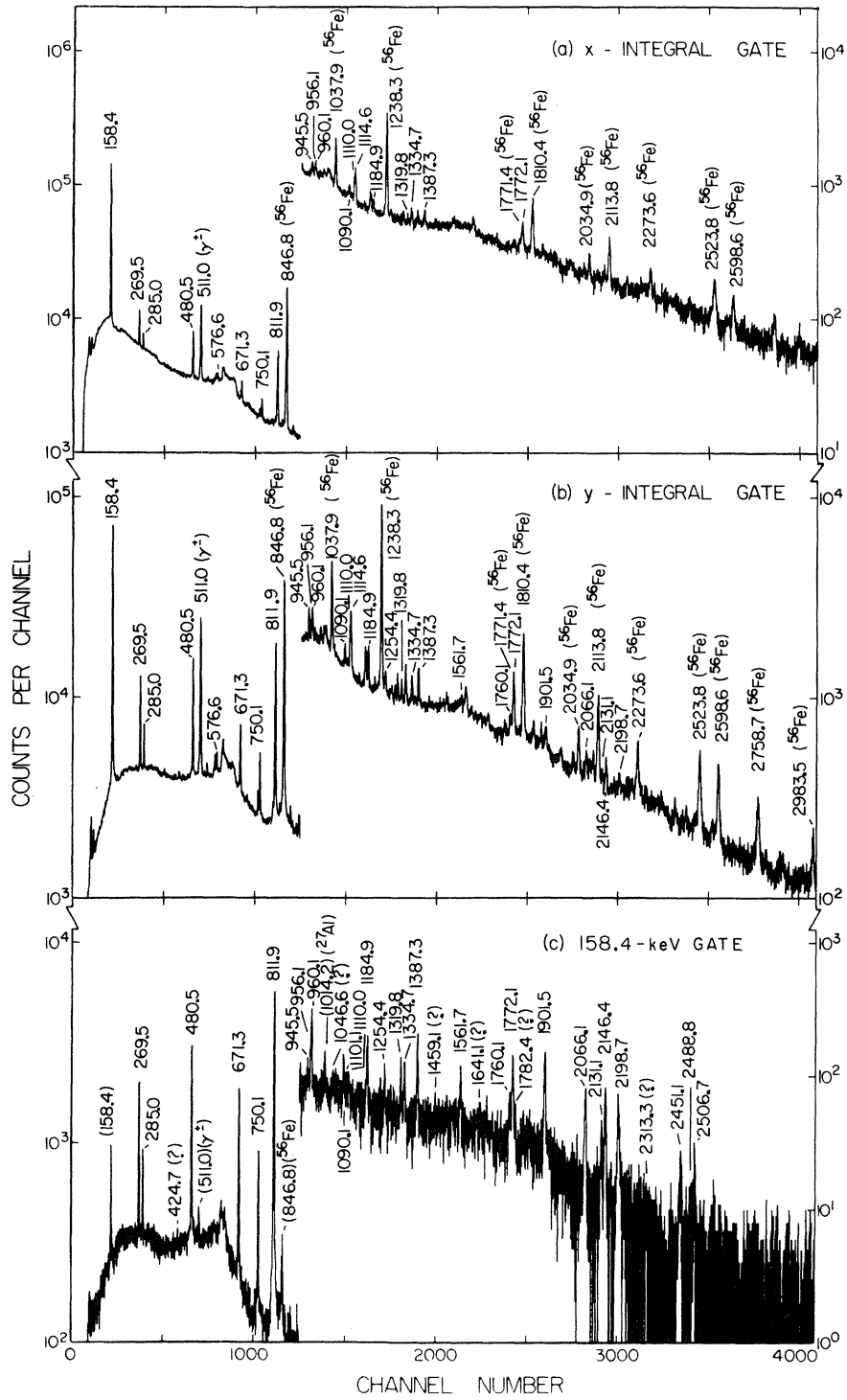


FIG. 5. Integral coincidence and representative gated spectra from the  $^{56}\text{Fe}(p,n\gamma\text{-}\gamma)^{56}\text{Co}$   $\gamma\text{-}\gamma$  coincidence experiment at  $E_p = 8.36$  MeV.  $\gamma$  rays labeled with a question mark, although they appear to be in coincidence, could not be placed in the decay scheme. Peaks in parentheses are believed to be from chance coincidences or insufficient background subtraction.



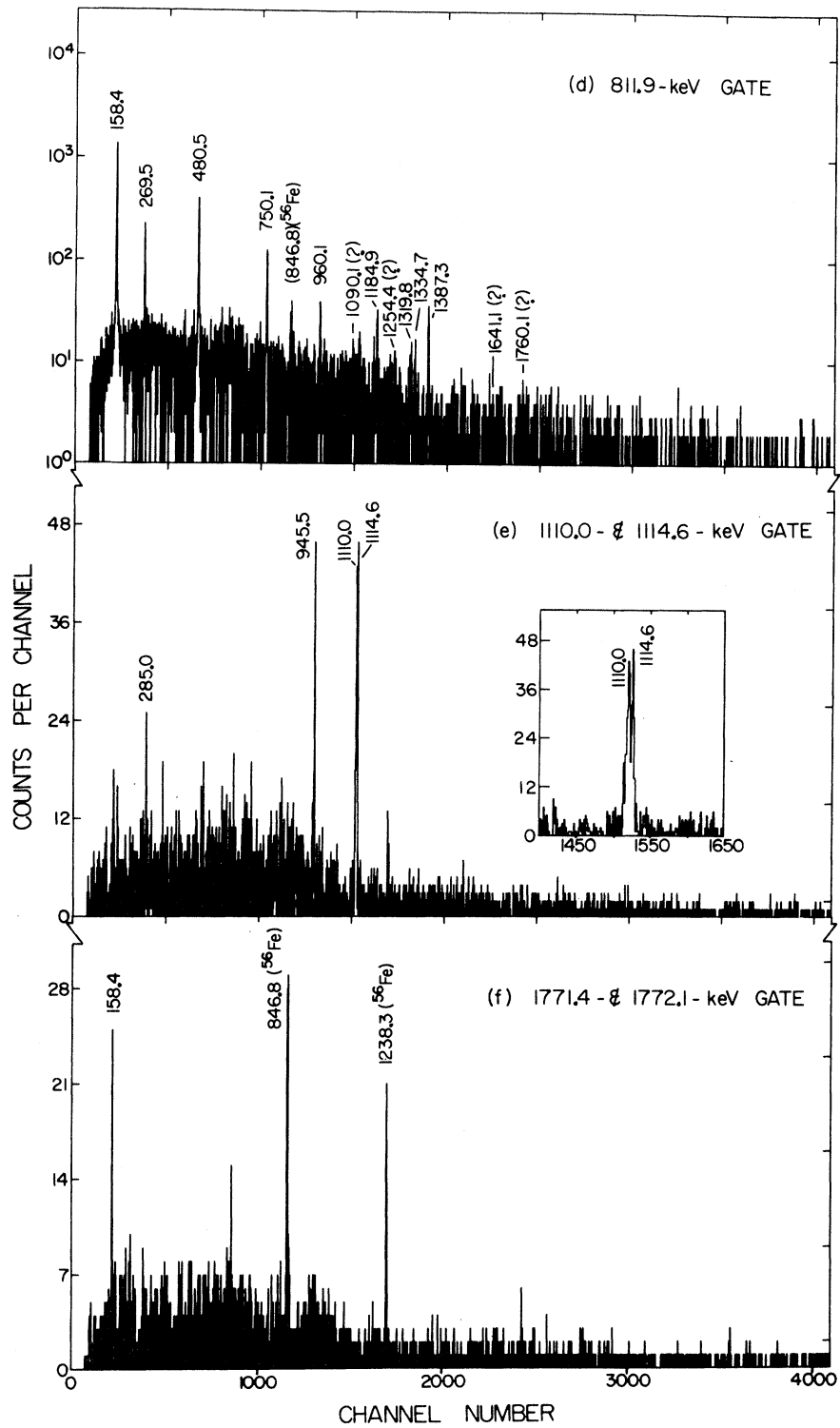


FIG. 5 (Continued)

fore assumed. This assumption is supported, however, by the even  $l$  transfers observed in the ( $d, \alpha$ ) experiment of Schneider and Daehnick<sup>9</sup> and in the ( $p, ^3\text{He}$ ) experiment of Bruge and Leonard,<sup>11</sup> and by shell-model considerations.<sup>28, 50</sup> In its simplest shell-model configuration,  $^{56}\text{Co}$  has two valence nucleons: a proton hole in the  $f_{7/2}$  orbit and a neutron in the  $p_{3/2}$  orbit. Since the three nearest orbits available for particle excitations ( $p_{3/2}$ ,  $f_{5/2}$ , and  $p_{1/2}$ ) have odd parities, all states formed with the required even number of valence nucleons will necessarily have a total even parity. The simplest shell-model states having odd parities that can be formed have particle configurations  $[(\pi d_{3/2})^{-1}(\nu p_{3/2})]$  and  $[(\pi f_{7/2})^{-1}(\nu g_{9/2})]$ . Because of the energy required for formation, such states would be expected at considerably higher excitations.

Because of the high Compton continuum and the large number of  $^{56}\text{Fe}$   $\gamma$  rays from the  $^{56}\text{Fe}(p, p'\gamma)$  reaction that occur in all singles spectra, ground-state transitions in  $^{56}\text{Co}$  having no coincidences and having energies greater than 2 MeV are difficult to identify. Thus, although some such ground-state transitions would be expected from states excited in the present experiments, none was positively identified. Also, because of these same reasons, branching ratios for those states above 1.8 MeV of excitation could not be determined.

#### B. $\gamma$ -Ray Excitation Functions

The  $\gamma$ -ray excitation functions were obtained with proton beams having energies ranging from 5.55 to 7.75 MeV. These beams were stepped in 100-keV intervals with the Western Michigan University tandem Van de Graaff. The target was the same  $^{56}\text{Fe}$  foil used in the coincidence studies and contributed approximately 40 keV to the energy spread of the proton beams. The  $\gamma$  rays from the  $^{56}\text{Fe}(p, n\gamma)^{56}\text{Co}$  reaction were detected with the 2.5%-efficient Ge(Li) detector (previously described) at approximately  $125^\circ$  [a zero of  $P_2(\cos\theta)$ ] from the beam direction (to minimize angular distribution effects) and at 5 cm from the target. The charge was collected and integrated in a shielded 90-cm-long, 8.3-cm-diam piece of lead-lined aluminum beam pipe.

Dead-time and amplifier pileup corrections, as well as run-to-run normalizations, were made by using the digitized output from a beam current integrator to trigger a Berkley Nucleonics Corporation model No. BH-1 tail-pulse generator. The pulser was in turn connected to the test input of the detector's preamplifier. The resulting pulser peak in the  $\gamma$ -ray spectrum was placed so as not to interfere with  $\gamma$ -ray peaks. Again, to preserve optimum resolution and symmetric peak shapes,

an ORTEC model No. 450 research amplifier was direct coupled to a Northern Scientific 100-MHz ADC. The  $\gamma$ -ray spectra were stored in 4096 channels with approximately 0.5 keV per channel in the Western Michigan University on-line PDP-15 computer. Typical run times were 50 min with counting rates of less than 6000 cps.

$\gamma$ -ray spectra that show the appearance and growth of the various  $^{56}\text{Co}$   $\gamma$  rays are displayed in Fig. 7. In addition to 17  $^{56}\text{Co}$   $\gamma$  rays previously identified from the coincidence experiments, a 1009.2-keV ground-state transition was identified. The approximate thresholds of the  $^{56}\text{Co}$   $\gamma$  rays were completely in agreement with their placement in the excited-state level scheme. The maximum beam energy of 7.75 MeV allowed identification of  $\gamma$  rays from states up to 2.26 MeV of excitation in  $^{56}\text{Co}$ .

The excitation functions for the first eight excited states of  $^{56}\text{Co}$ , measured to a maximum excitation of 2.26 MeV, are shown in Fig. 8. For each data point the total neutron population of the state was determined by subtracting the intensities of all the  $\gamma$  rays feeding the state (where appropriate) from the intensities of all the  $\gamma$  rays deexciting the state. Internal-conversion corrections were neglected since they were small in comparison to experimental errors. (The largest correction would be 1% for the 158.4-keV  $M1$  transition.<sup>2</sup>) The  $\gamma$ -ray intensities were determined from the peak areas obtained using SAMPO<sup>32</sup> and the detector's relative efficiency curve. The neutron population of each state at each beam energy was normalized by dividing by the pulser peak area.

The most noticeable features of the excitation functions are the large fluctuations. The maximum experimental error associated with any given point is 12%, whereas the point-to-point fluctuations average 15% and some are as high as 100%. Since the fluctuations do not correlate in sign and magnitude from state to state, it is unlikely that they originate from an incorrect experimental technique. Hausman, Humes, and Seyler<sup>51</sup> observed this same phenomenon in their low-energy  $^{48}\text{Ti}(p, p'\gamma)$  experiment (there a CN excitation of  $\approx 11.7$  MeV was achieved). Since their fluctuations persisted from angle to angle and were approximately 100 keV wide, they suggested that the peaks resulted neither from Ericson-type fluctuations nor isolated resonances. Since the statistical CN excitation-function predictions agreed well both in shape and in absolute magnitude with their data averaged over 200-keV energy intervals, they further concluded that an experimental energy spread of 200 keV would have resulted in good statistical averaging, whereas their actual 50-keV spread was too small.

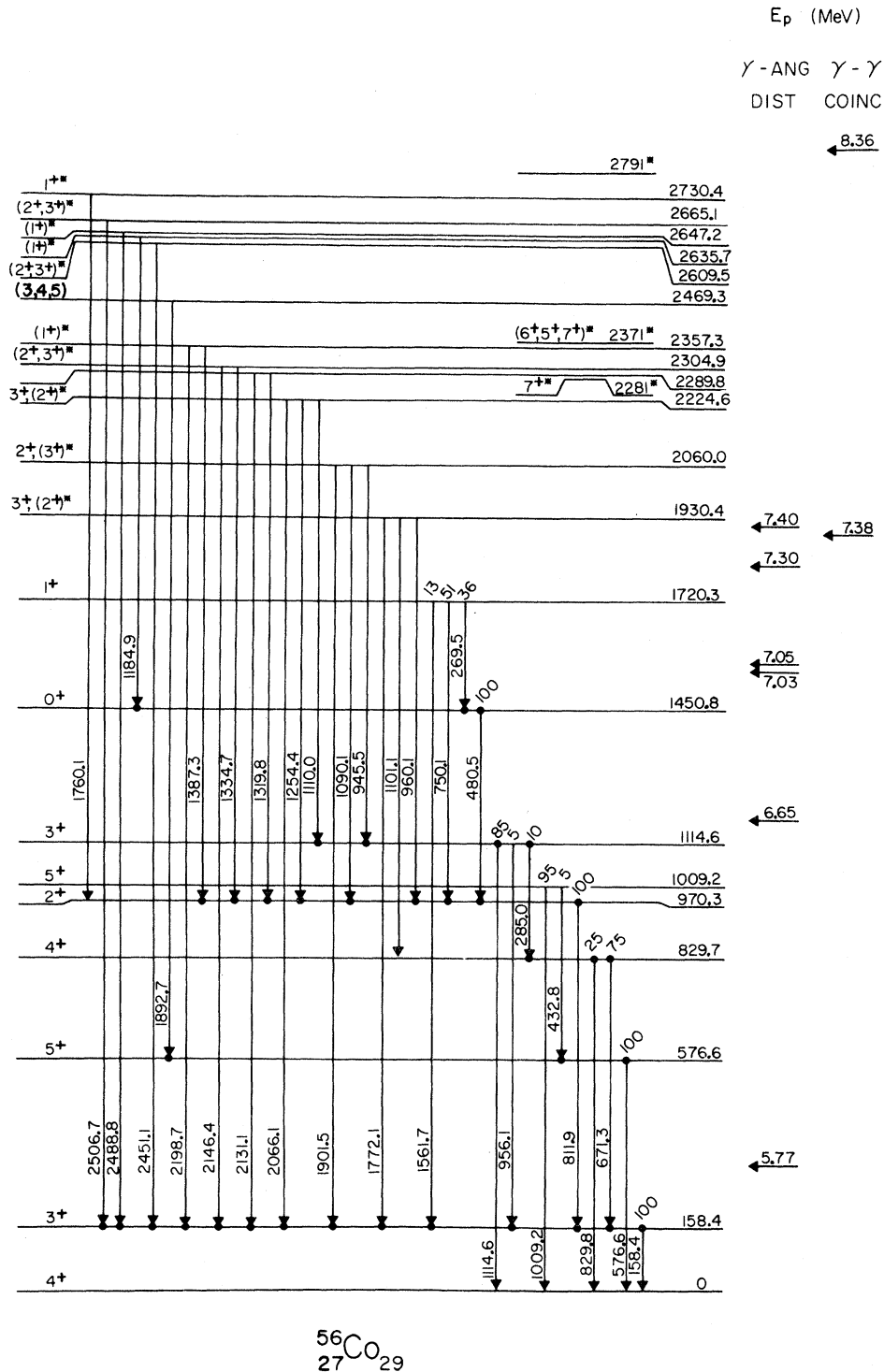


FIG. 6. The  $\gamma$ -ray decay scheme for excitations of  $^{56}\text{Co}$ . The  $\gamma$ -ray energies and branching ratios were measured using the  $^{56}\text{Fe}(p, n\gamma)^{56}\text{Co}$  reaction. The arrows on the right indicate the maximum possible excitations for the proton energies of the  $\gamma$ - $\gamma$  coincidence and  $\gamma$ -ray angular distribution experiments. The spins, parities, and level energies labeled with an asterisk are from Ref. 9, while the remaining values were determined from  $^{56}\text{Fe}(p, n\gamma)^{56}\text{Co}$  experiments and are discussed in Sec. IV. Dots denote observed coincidence relationships between  $\gamma$ -ray transitions entering and leaving a state.

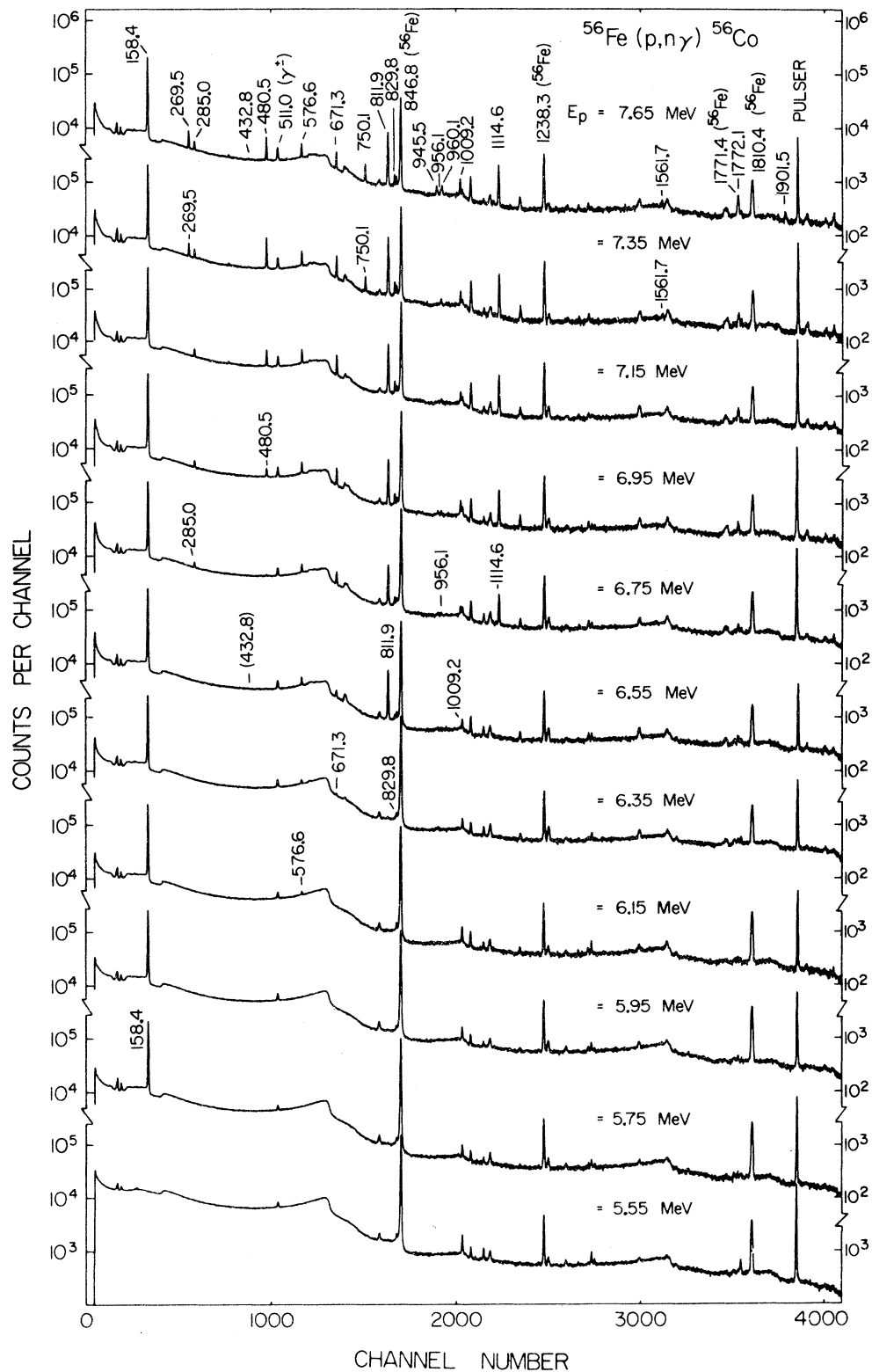


FIG. 7.  $\gamma$ -ray spectra from the excitation function measurements. The first appearances of the various  $^{56}\text{Co}$   $\gamma$  rays are labeled. Each spectrum was counted until one channel of the 158.4-keV peak reached  $2^{18}$  counts. Proton energies given are in the laboratory system.

TABLE IV. Results of two parameter  $\gamma$ - $\gamma$  coincidence experiments from the  $^{56}\text{Fe}(p, n\gamma)\text{Co}$  reaction.

Gate $\gamma$ ray (keV)	Coincident $\gamma$ rays <sup>a</sup> (keV)
158.4	269.5(4.9), 285.0(1.8), 424.7 <sup>b</sup> (0.45), 480.5(20), 671.3(21), 750.1(12), 811.9(=100), 945.5(0.74), 956.1(1.6), 960.1(5.3), 1046.6 <sup>b</sup> (0.97), 1090.1(2.1), 1101.1(1.1), 1110.0(1.1), 1184.9(4.7), 1254.4(2.1), 1319.8(3.0), 1334.7(3.3), 1387.3(6.3), 1459.1 <sup>b</sup> (1.2), 1561.7(4.0), 1641.1 <sup>b</sup> (1.1), 1760.1(2.7), 1772.1(8.0), 1782.4 <sup>b</sup> (1.3), 1901.5(10), 2066.1(7.0), 2131.1(4.0), 2146.4(9.4), 2198.7(7.1), 2313.3 <sup>b</sup> (0.89), 2451.1(2.7), 2488.8(1.0), 2506.7(3.1)
269.5	158.4(16), 480.5(85), 811.9(=100)
285.0	158.4(13), 671.3(=100), 829.8(32), 945.5(16), 1110.0(23)
480.5	158.4(16), 269.5(17), 811.9(=100), 1184.9(16)
576.6	432.8(11), 1892.7(=100)
671.3	158.4(=100), 285.0(51), 945.5 <sup>c</sup> (24)
750.1	158.4, 811.9
811.9	158.4(73), 269.5(23), 480.5(=100), 750.1(66), 960.1(32), 1090.1 <sup>c</sup> , 1184.9(26), 1254.4 <sup>c</sup> , 1319.8(10), 1334.7(13), 1387.3(33), 1641.1 <sup>c</sup> , 1760.1 <sup>c</sup>
829.8	285.0
945.5	158.4(5.2), 285.0(12), 671.3(23), 1114.6(=100)
956.1 and 960.1	158.4, 811.9
1090.1	158.4, 811.9
1110.0 and 1114.6	285.0(7.1), 945.5(70), 1110.0(=100), 1114.6(84)
1184.9	158.4(65), 480.5(=100), 811.9(67)
1254.4	158.4, 811.9
1319.8	158.4, 811.9
1334.7	158.4, 811.9
1387.3	158.4, 811.9
1561.7	158.4
1760.1	158.4, 811.9 <sup>c</sup>
1772.1	158.4
1782.4	158.4 <sup>c</sup>
1901.5	158.4
2066.1	158.4
2131.1	158.4
2146.4	158.4

<sup>a</sup> Numbers in parentheses following the  $\gamma$ -ray energies represent the  $\gamma$ -ray relative intensities (normalized to 100 for the most intense peak) observed in that particular gated spectrum. It should be carefully noted that since these numbers are highly geometry-dependent (because of angular correlation effects), they are presented solely as a crude indication of the peak intensities that one might expect to observe in a similar experiment.

<sup>b</sup> These  $\gamma$  rays seem to be in coincidence with the gated  $\gamma$  ray but could not be placed explicitly in the excited-state level scheme.

<sup>c</sup> These  $\gamma$ -ray peaks did not have sufficient statistics to warrant the claim of a definite coincidence.

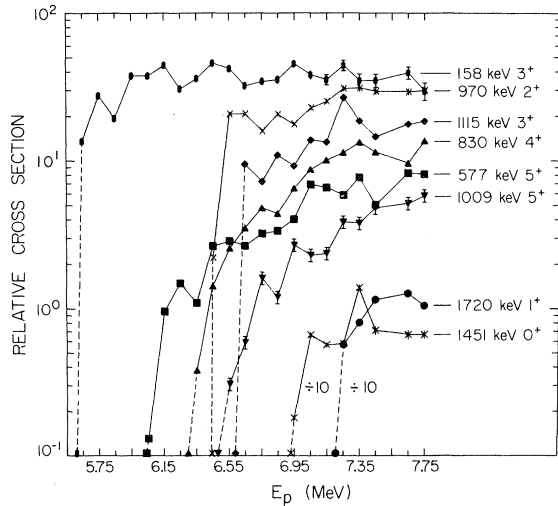


FIG. 8. Excitation functions for the first eight excited states of  $^{56}\text{Co}$ . The data were taken at  $125^\circ$ , a zero of  $P_2(\cos\theta)$ , in order to minimize angular distribution effects. Neutron feedings were computed for each level from the  $\gamma$ -ray intensity imbalances and then were normalized from run to run (as described in the text) to obtain the relative cross sections. The thresholds were calculated using  $Q = -5.357$  MeV for the ground state (Ref. 47) and are connected to the first nonzero data points with dotted lines. Solid lines connect the data to guide the eye. Where not visible, error bars are smaller than the data-point symbol.

In similar experiments with  $A \approx 60$  and CN excitations of 10–15 MeV, Lee and Schiffer<sup>52</sup> observed fluctuations on the order of 2–3 times the experimental resolution. They suggested that the assumption of complete randomness of the statistical CN theory may be invalid and that some residual interactions may cause clustering of strong levels that give rise to the gross fluctuations. No conclusions can be drawn from the present experiment concerning the above suggestions other than to say that similar gross fluctuations have been observed.

From level-density studies by Huizenga and Katsanos,<sup>53</sup> the average level spacing in  $^{57}\text{Co}$  (assuming similarity to  $^{57}\text{Fe}$  for which empirical parameters are known) at a CN excitation of about 12 MeV (corresponding to a beam energy of about 6 MeV) is expected to be 0.03 keV. Thus, the energy spread of 40 keV is predicted to overlap  $\approx 1300$  CN states of mixed spin and parity in the present experiment. The overlap predicted for  $^{49}\text{V}$  in the experiment of Hausman *et al.*,<sup>51</sup> was 1800 CN states. Thus, the conclusion here is similar to that of Hausman *et al.*,<sup>51</sup> namely, that since the agreement between experimental and theoretical cross-section ratios and  $\gamma$ -ray angular distributions is so good (see below), the statistical CN theory reasonably describes the situation even

though complete statistical averaging is not achieved.

In order to compare the excitation functions with the predictions of the statistical CN theory, experimental and theoretical cross sections for the various excited states of  $^{56}\text{Co}$  are plotted in Fig. 9 as ratios with respect to those for the 158.4-keV first excited state. As is shown in Fig. 9 the theoretically predicted cross sections vary as a function of the spin and parity of the final excited state. This fact can be seen most easily from the following expression for the total cross section<sup>54</sup>:

$$\sigma = \frac{\lambda^2}{8\pi} \sum_{j_1, j_2} (2J_1 + 1)\tau,$$

where  $\lambda$  is the wavelength of the incoming proton,  $J_1$  is the spin of the intermediate state in the compound nucleus, and  $\tau$  is the penetrability term. The penetrability  $\tau$  is determined from the following expression<sup>54</sup>:

$$\tau = \frac{T_{l_1 j_1}(E_1) T_{l_2 j_2}(E_2)}{\sum T_{l j}(E)},$$

where the  $T_{l j}(E)$ 's are the various particle transmission coefficients which depend upon the particle's center-of-mass energy  $E$ , and orbital and total angular momentum  $l$  and  $j$ , respectively. The sum in the denominator extends over all open channels by which the intermediate CN state can decay.

The sum in the total cross-section expression is made over all possible values of  $j_1$  and  $j_2$ , which are the total angular momentum of the incoming protons and outgoing neutrons, respectively. Since this sum involves the spin of the intermediate CN state, parity conservation and the angular-momentum coupling rules require a different sum over the numerical  $\tau$  values for each possible final excited-state spin and parity. Since the target has  $J^\pi = 0^+$  and since the outgoing neutrons are mostly  $l=0$ , low- (high-) spin final states are reached predominantly through low- (high-) spin intermediate states which are in turn reached by low- (high-) angular-momentum protons. At these bombarding energies (5.5–7.5 MeV), the incoming protons are predominantly  $l=2$ . Thus, the cross sections are expected to be largest for  $J$  values of 1, 2, or 3. The division of the cross section to each final state by that to the 158.4-keV state (at the same proton energy), removes the absolute normalization and thus makes the comparison of the experimental and theoretical values quantitative. The interpretation of Fig. 9 in regard to spin assignments is discussed in Sec. IV.

The theoretical cross sections used above and the theoretical angular distribution parameters  $A_2^*$  and  $A_4^*$  were calculated using the statistical CN

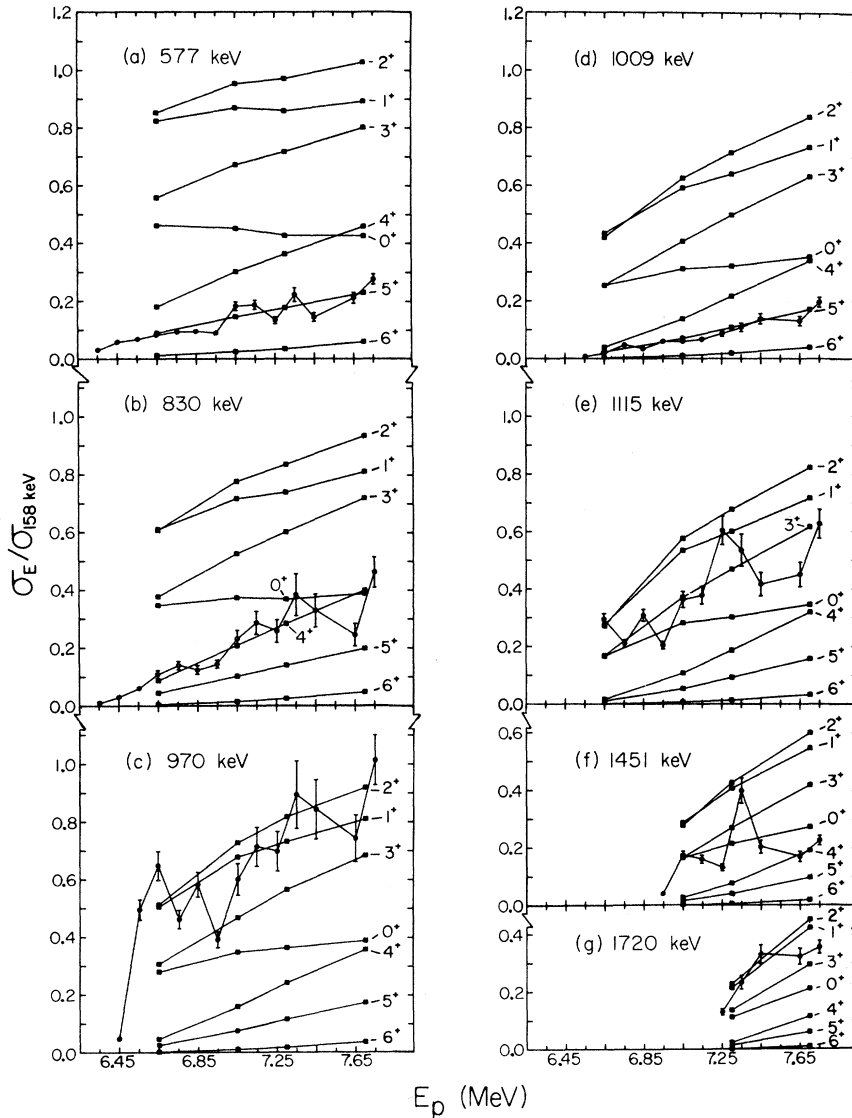


FIG. 9. Experimental and theoretical cross-section ratios. The ratios are taken with respect to the 158.4-keV first excited state. Error bars identify the data (lines connecting the data are to guide the eye). MANDY predictions for selected beam energies are shown for  $J^\pi = 0^+, \dots, 6^+$ . A  $J^\pi = 3^+$  for the 158.4-keV state was used as explained in the text. Straight lines connecting the theoretical points approximate expected smooth curves.

computer code MANDY written by Sheldon, Gantenbein, and Strang.<sup>54</sup> MANDY requires as input the transmission coefficients  $T_{ij}(E)$  for all open entrance and exit channels. These coefficients were computed with a modified version of the optical-model code ABACUS-II.<sup>55</sup> For the real spin-independent part of the nuclear potential, the usual Woods-Saxon form was used; for the imaginary part, the derivative of the Woods-Saxon form was used; and for the spin-orbit part, the Thomas form was used.

The proton transmission coefficients were calculated using the local optical-model parameters list-

ed in Table V. These parameters were determined by Perey<sup>56</sup> from elastic scattering data in the 9–22-MeV range. It was assumed that the explicit energy dependence would allow the use of these parameters at energies as low as 4 MeV. These same parameters were used quite successfully by Hausman *et al.*<sup>51</sup> in their  $^{48}\text{Ti}$  study.

The neutron transmission coefficients were calculated using the local equivalent optical-model parameters of Perey and Buck<sup>57</sup> listed in Table V. Again it was assumed that the explicit energy dependence would allow the use of these parameters at energies as low as 40 keV and as high as 1.8

TABLE V. Form of the optical-model potential and parameters used in the calculations of transmission coefficients. The Coulomb potential,  $V_C(r)$ , is that due to a uniformly charged sphere of radius  $1.25A^{1/3}$  (fm). The parameter  $E$  is the center-of-mass energy of the nucleon in MeV:

$$V = V_C(r) - V_0 \frac{1}{1 + e^{(r-R)/a}} + iW_D \frac{d}{dr} \frac{4a'}{1 + e^{(r-R')/a'}} + \left( \frac{\hbar}{m_\pi c} \right)^2 \frac{V_{so}}{r} l \cdot \sigma \frac{d}{dr} \frac{1}{1 + e^{(r-R)/a}}; \quad R = r_0 A^{1/3}, \quad R' = r'_0 A^{1/3}.$$

Nucleon	$V_0$ (MeV)	$W_D$ (MeV)	$r_0$ (fm)	$r'_0$ (fm)	$a$ (fm)	$a'$ (fm)	$V_{so}$ (MeV)
Proton <sup>a</sup>	$46.7 - 0.32E + ZA^{-1/3}$	11	1.25	1.25	0.65	0.47	7.5
Neutron <sup>b</sup>	$48.0 - 0.29E$	10	1.25	1.25	0.65	0.47	7.5

<sup>a</sup> The proton parameters, except  $V_{so}$ , are from Ref. 56.

<sup>b</sup> The neutron parameters and the proton  $V_{so}$  are from Ref. 57.

MeV. These neutron and proton parameters were also used by Sheldon.<sup>58</sup> The depth of the real spin-orbit potential for both neutrons and protons was taken as 7.5 MeV, which is the local equivalent to the nonlocal value used by Perey and Buck.

14 inelastic proton channels and all known open neutron channels were included in each of the MANDY calculations. The spins and energies for the proton channels are from  $^{56}\text{Fe}(n, n'\gamma)$  work by Armitage *et al.*<sup>48</sup> There are many more open proton channels than were included; however, it was felt that they could be safely ignored, as the exit proton energies involved are well below the 5.39-MeV Coulomb barrier. These low-energy protons also have much less phase space available to them. A comparison of predicted and measured absolute cross sections is made later in Sec. III D.

Since the theoretical cross-section predictions involve the use of estimated optical-model parameters (in determining the penetrabilities), systematic errors in these predictions are possible. The internal consistency of the present experimental results and the agreement of some of the results with previously known quantities indicate that these possible systematic errors are minimal. No attempt was made to vary any of the optical-model parameters in the theoretical calculations.

The errors assigned to the experimental points of Figs. 8 and 9 arise from uncertainties in three different quantities: (1) the  $\gamma$ -ray peak areas, (2) the detector relative  $\gamma$ -ray efficiency corrections, and (3) the run-to-run normalizations. The  $\gamma$ -ray peak area uncertainties result from the inherent statistical error associated with a nuclear decay process as well as from systematic analysis errors particularly in the determination of background. The latter is felt to be an often neglected but very important source of error. An estimate of the combined error (for each peak) was made by comparison with the  $\gamma$ -ray angular distribution data and is described in the next section. (The  $\gamma$ -ray spectra of both experiments were quite sim-

ilar.) The resulting estimated peak-area errors varied from 1.5 to 10% and in all cases were larger than the statistical errors. The uncertainties in the relative efficiency corrections were estimated to be between 3 and 5% (depending upon the  $\gamma$ -ray energy) by comparing graphically several possible fits to the experimental detector relative efficiency curve. Although systematic errors could enter here, they would be difficult to estimate. The uncertainties in the run-to-run normalizations were estimated to be between 0.5 and 1% (depending upon the pulser-peak area). Special care was taken to arrange the geometry to insure against any additional systematic errors associated with beam loss or secondary electron emission and subsequent loss of charge from the Faraday cup arrangement.

### C. $\gamma$ -Ray Angular Distributions

Proton beams of 5.77, 6.65, 7.03, 7.05, 7.30, and 7.40 MeV from the MSU cyclotron were used to bombard a piece of the previously described enriched  $^{56}\text{Fe}$  foil. A thin strip of foil measuring 1 mm by 10 mm was carefully positioned on the axis of rotation of a high angular precision goniometer.<sup>59</sup> Thus, only when the beam passed through the axis of rotation could  $^{56}\text{Co}$   $\gamma$  rays be produced. A diagram of the scattering chamber geometry is shown in Fig. 10.

The 2.5%-efficient Ge(Li) detector was rigidly mounted on the goniometer arm with the face of the detector 12.7 cm from the target. The detector subtended approximately  $10^\circ$  of arc. A semi-circle of 99.999% pure lead with a thickness of  $0.419 \pm 0.013$  mm was placed 5 cm from the target. Since this thickness of lead was capable of stopping 12-MeV protons, angular distributions all the way to  $0^\circ$  could be taken for all bombarding energies. Also,  $\gamma$  rays from reactions with the lead, although present, were minimal since the beam energies used were considerably below the 11.8-



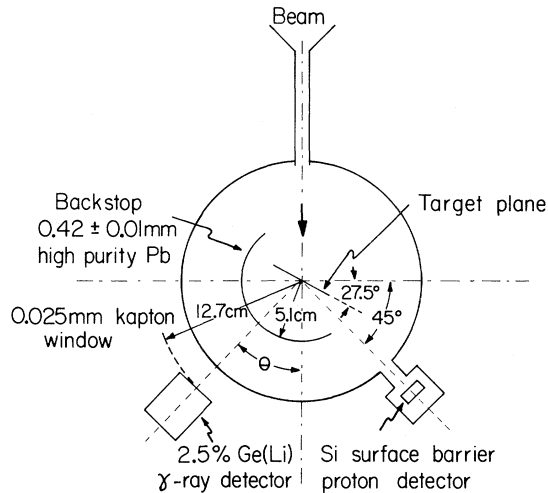


FIG. 10. Geometry for the in-beam  $\gamma$ -ray angular distribution measurements. The monitor and target angles were held fixed throughout all of the measurements.

MeV Coulomb barrier for lead. As a precaution, all of the beam line near the detector was carefully lined with clean lead to eliminate any  $\gamma$  rays from beam-induced reactions with the aluminum beam pipe.

An electronic setup similar to that used to take the excitation-function data was used to compensate for pileup and dead-time effects caused by changing  $\gamma$ -ray counting rates due to beam current fluctuations and an increase of  $\gamma$ - and x-ray intensities from the lead beam stop as  $0^\circ$  was approached. Here the pulse generator was triggered by elastically scattered proton counts provided by a properly collimated silicon surface-barrier detector held rigidly in place at  $-45^\circ$  with respect to the beam direction. Since the total number of protons scattered into a given solid angle is directly proportional to the total integrated beam current that has passed through the target, correct normalization for the distributions taken at 5.77, 6.65, 7.05, and 7.40 MeV was then provided by simply dividing  $\gamma$ -ray peak areas by the pulser peak area. Once isotropy of the 480.5-keV  $\gamma$ -ray transition was well established in the 7.05- and 7.40-MeV angular distributions, this transition was used as an internal normalization for the angular distributions taken at 7.03 and 7.30 MeV (the tail-pulse generator was not available).

The data were stored in 4096 channels with approximately 0.5 keV per channel through a Northern Scientific 50-MHz ADC interfaced to the MSU cyclotron's XDS  $\Sigma$ -7 computer.<sup>31</sup> The spectra (at the appropriate beam energies) are very similar to those presented in Fig. 7. Typically, spectra were accumulated for 1 h between changes of angle and usually angular distributions contained 20

points in  $10^\circ$  intervals taken in random order over the angular range of 0 to  $90^\circ$ . Duplication of most points increased confidence in the data.

The spectra were analyzed off line using the computer code SAMPO<sup>32</sup> which allowed analysis consistency and which allowed some of the  $\gamma$ -ray peaks to be stripped from weak adjacent back-ground peaks. After normalization of  $\gamma$ -ray peak areas, least-squares fits to the experimental  $\gamma$ -ray angular distributions using the computer code GADFIT<sup>60</sup> were made to the equation:

$$W(\theta) = A_0 [1 + A_2^* P_2(\cos\theta) + A_4^* P_4(\cos\theta)].$$

The parameters extracted from the fit are  $A_0$ ,  $A_2^*$ , and  $A_4^*$ , where  $A_0$  is the intensity integrated over all solid angles. By correcting these integrated intensities for the relative detector efficiency and absorption in the lead semicircle, branching ratios having all angular dependence removed were obtained. These branching ratios agreed well with those obtained from the excitation function data.

The branching ratios presented in Fig. 6 and listed in Table VIII of Sec. V are averages of the two experiments. The effects on the angular distribution of the nonzero solid angular acceptance of the detector were found to be negligible. The  $\gamma$ -ray angular distributions taken at beam energies of 5.77, 6.65, 7.05, and 7.30 MeV and selected  $\gamma$ -ray angular distributions taken at 7.40 MeV are shown in Fig. 11, while the measured  $A_2^*$  and  $A_4^*$  values for all beam energies are listed in Table VI.

For each angular distribution measured, theoretical  $A_2^*$  and  $A_4^*$  coefficients as functions of the mixing ratio  $\delta$  were generated from MANDY for a particular final spin and an assortment of initial spins. An example of these  $\delta$  ellipses is shown in Fig. 12. The functional form of  $W(\theta)$  using these predicted values of  $A_2^*$  and  $A_4^*$  (as a function of  $\delta$ ) was then compared with the experimental data to determine the  $\chi^2$  per degree of freedom (reduced  $\chi^2$ ) for the fit. For reduced  $\chi^2$  to be meaningful, however, "accurate" uncertainties must be assigned to the data. Since two points were taken at each angle it was found that the purely statistical uncertainties rarely caused overlapping error bars. This fact would indicate that these uncertainties were underestimating the true uncertainties. For the  $\gamma$ -ray angular distribution measurements, the major uncertainties are in the  $\gamma$ -ray peak areas and the angle-to-angle normalizations (pulser peak areas). As indicated in the previous section, systematic errors (primarily in the background determination) are very important in the case of the  $\gamma$ -ray peak areas. Since it was felt that these systematic errors could not be "accurately" estimated *a priori*, the following approach was taken.

The uncertainties for each of the data points were adjusted during the determination of the experimental  $A_2^*$  and  $A_4^*$  coefficients to make the reduced  $\chi^2$  for the best fit to be approximately one. This condition yields accurate uncertainties provided the form of the fitting function  $W(\theta)$  is correct. Since direct interaction effects are expected to be small at the beam energies used, the even-order Legendre polynomial series used in  $W(\theta)$  is probably valid. The uncertainties determined in this manner varied from 1.5 to 10%. In all cases these uncertainties were larger than the combined statistical errors of the  $\gamma$ -ray peak areas and the pulser peak areas.

The values of reduced  $\chi^2$  were determined from

the theoretical  $A_2^*$  and  $A_4^*$  coefficients, the experimental  $\gamma$ -ray angular distribution, and the data uncertainties (determined as described above), and were plotted against  $\arctan \delta$ . Some representative plots are shown in Fig. 13. (The remaining plots can be found in Ref. 49.) All relevant spin and parity values have been included in the plots, although in each case several of them can be eliminated on the basis of cross-section ratios as discussed in the next section. The ordinate is labeled "relative  $\chi^2$ " instead of "reduced  $\chi^2$ " because of the manner in which the uncertainties were determined. It should be noted that a pronounced minimum in relative  $\chi^2$  will only be approximately unity if the theoretical  $\delta$  ellipse passes through the experi-

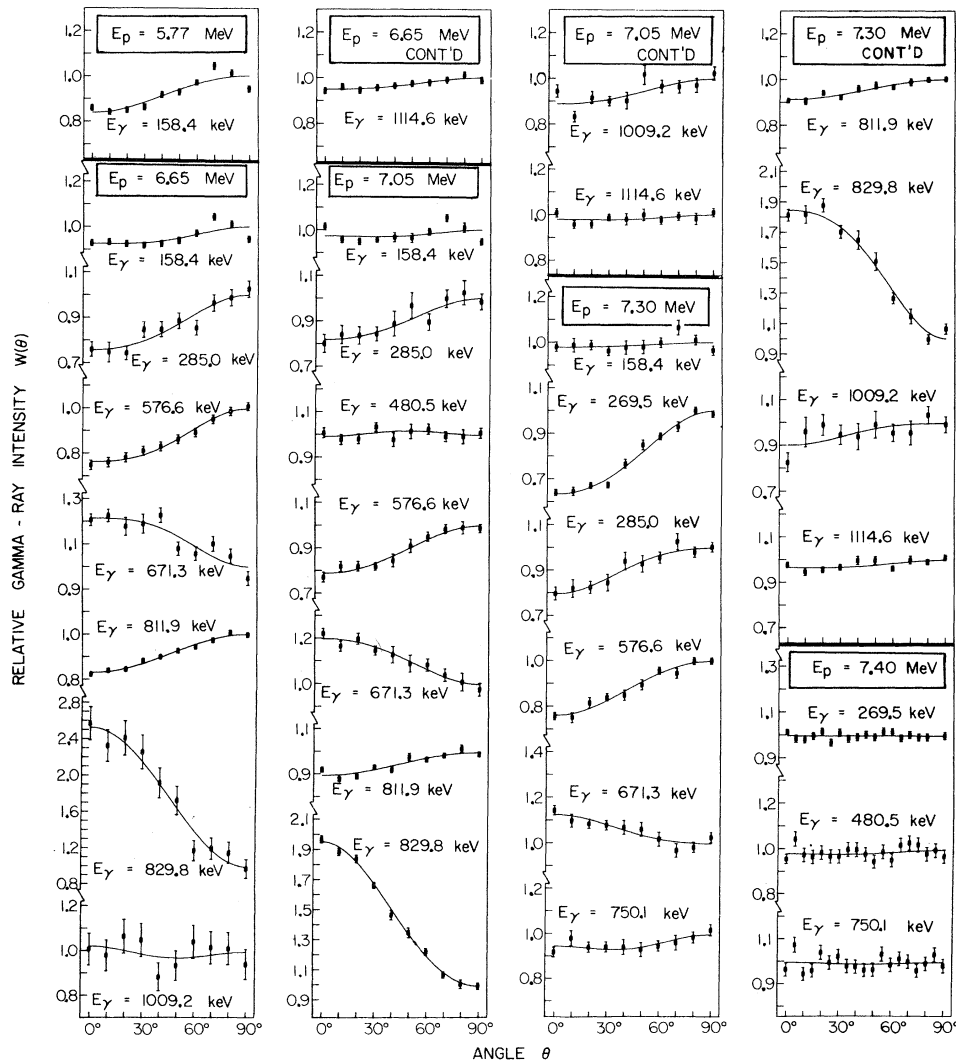


FIG. 11. Angular distributions of  $^{56}\text{Co}$   $\gamma$  rays taken at  $E_p = 5.77, 6.65, 7.05, 7.30,$  and  $7.40$  MeV. The solid lines through the data represent least-squares fits using the equation for  $W(\theta)$  given in the text.  $W(\theta)$  has been normalized to 1 at  $90^\circ$ . Except for the  $E_p = 7.40$  MeV case, two experimental points were taken at each angle; only their weighted average is presented.

TABLE VI. Experimental  $\gamma$ -ray angular distribution fitting parameters  $A_2^*$  and  $A_4^*$  and the associated  $\gamma$ -ray multipole mixing ratio  $\delta$ . The fitting parameters and mixing ratio are defined in the text. The errors assigned to both the  $A_2^*$  and  $A_4^*$  coefficients represent plus or minus 1 standard deviation. The ranges of  $\delta$  were determined from these coefficients as described in the text.

$E_p$ (MeV)	$E_\gamma$ (keV)	$A_2^*$	$A_4^*$	$\delta$
5.77	158.4	$-0.110 \pm 0.018$	$-0.008 \pm 0.020$	$-0.034 \leq \delta \leq -0.006$
6.65	158.4	$-0.059 \pm 0.015$	$0.019 \pm 0.019$	$-0.048 \leq \delta \leq -0.010^a$
	285.0	$-0.190 \pm 0.076$	$0.027 \pm 0.092$	$-0.020 \leq \delta \leq 0.088$
	576.6	$-0.191 \pm 0.042$	$0.037 \pm 0.053$	$0.022 \leq \delta \leq 0.072^a$
	671.3	$0.146 \pm 0.060$	$-0.038 \pm 0.067$	$0.221 \leq \delta \leq 0.304^a$
	811.9	$-0.121 \pm 0.010$	$0.001 \pm 0.012$	$0.015 \leq \delta \leq 0.035$
	829.8	$0.673 \pm 0.353$	$0.005 \pm 0.432$	$-0.092 \leq \delta \leq 1.145^a$
	1009.2	$-0.002 \pm 0.346$	$0.035 \pm 0.410$	$-0.024 \leq \delta \leq 0.361$
	1114.6	$-0.038 \pm 0.025$	$0.006 \pm 0.030$	$-0.093 \leq \delta \leq -0.056$
7.03	158.4	$-0.013 \pm 0.009$	$0.011 \pm 0.009$	b
	285.0	$-0.122 \pm 0.038$	$0.029 \pm 0.047$	$-0.028 \leq \delta \leq 0.039$
	576.6	$-0.178 \pm 0.016$	$0.023 \pm 0.023$	$0.041 \leq \delta \leq 0.061^a$
	671.3	$0.141 \pm 0.023$	$-0.020 \pm 0.033$	$0.253 \leq \delta \leq 0.290^a$
	811.9	$-0.066 \pm 0.010$	$0.003 \pm 0.012$	
		$-0.085 \pm 0.013^c$	$0.004 \pm 0.015^c$	$0.005 \leq \delta \leq 0.040^c$
	829.8	$0.517 \pm 0.055$	$-0.086 \pm 0.068$	d
	1009.2	$-0.080 \pm 0.072$	$-0.006 \pm 0.089$	$0.070 \leq \delta \leq 0.154$
1114.6	$-0.014 \pm 0.028$	$0.000 \pm 0.034$	$-0.116 \leq \delta \leq -0.064$	
7.05	158.4	$-0.024 \pm 0.012$	$0.012 \pm 0.018$	b
	285.0	$-0.137 \pm 0.075$	$0.015 \pm 0.100$	$-0.047 \leq \delta \leq 0.084$
	480.5	$0.002 \pm 0.027$	$-0.020 \pm 0.034$	$\delta = 0.0^e$
	576.6	$-0.158 \pm 0.021$	$0.009 \pm 0.029$	$0.050 \leq \delta \leq 0.076^a$
	671.3	$0.128 \pm 0.026$	$-0.014 \pm 0.031$	$0.241 \leq \delta \leq 0.282^a$
	811.9	$-0.073 \pm 0.009$	$-0.001 \pm 0.011$	
		$-0.090 \pm 0.011^c$	$-0.001 \pm 0.013^c$	$0.014 \leq \delta \leq 0.044^c$
	829.8	$0.475 \pm 0.043$	$0.038 \pm 0.061$	$0.337 \leq \delta \leq 0.467^a$
1009.2	$-0.082 \pm 0.069$	$0.008 \pm 0.088$	$0.071 \leq \delta \leq 0.151$	
1114.6	$-0.017 \pm 0.028$	$0.009 \pm 0.035$	$-0.113 \leq \delta \leq -0.061$	
7.30	158.4	$-0.015 \pm 0.015$	$0.002 \pm 0.018$	b
	269.5	$-0.296 \pm 0.023$	$0.030 \pm 0.031$	$\delta = 0.0^e$
	285.0	$-0.134 \pm 0.055$	$-0.025 \pm 0.076$	$-0.022 \leq \delta \leq 0.088$
	576.6	$-0.169 \pm 0.024$	$-0.008 \pm 0.032$	$0.040 \leq \delta \leq 0.070^a$
	671.3	$0.074 \pm 0.030$	$0.014 \pm 0.038$	$0.198 \leq \delta \leq 0.245^a$
	750.1	$-0.053 \pm 0.043$	$0.033 \pm 0.055$	$-22.7 \leq \delta \leq -2.91^f$ or $-0.041 \leq \delta \leq 0.251$
	811.9	$-0.060 \pm 0.008$	$0.000 \pm 0.011$	b
	829.8	$0.453 \pm 0.071$	$-0.086 \pm 0.091$	$0.142 \leq \delta \leq 0.715^a$
	1009.2	$-0.061 \pm 0.106$	$-0.017 \pm 0.144$	$0.059 \leq \delta \leq 0.186$
	1114.6	$-0.027 \pm 0.026$	$0.008 \pm 0.034$	$-0.102 \leq \delta \leq -0.047$
1561.7	$0.082 \pm 0.742$	$-0.070 \pm 1.074$	g	
7.40	158.4	$-0.028 \pm 0.009$	$0.016 \pm 0.009$	b
	269.5	$-0.018 \pm 0.025$	$0.006 \pm 0.029$	$\delta = 0.0^e$
	285.0	$-0.066 \pm 0.142$	$-0.006 \pm 0.163$	$-0.186 \leq \delta \leq 0.107$
	480.5	$-0.002 \pm 0.006$	$-0.001 \pm 0.007$	$\delta = 0.0^e$
	576.6	$-0.169 \pm 0.017$	$0.014 \pm 0.021$	$0.044 \leq \delta \leq 0.065^a$
	671.3	$0.087 \pm 0.021$	$-0.016 \pm 0.025$	$0.215 \leq \delta \leq 0.248^a$
	750.1	$-0.006 \pm 0.034$	$0.007 \pm 0.040$	$-4.30 \leq \delta \leq -1.95^h$ or, $-0.187 \leq \delta \leq 0.062^h$

TABLE VI (Continued)

$E_p$ (MeV)	$E_\gamma$ (keV)	$A_2^*$	$A_4^*$	$\delta$
7.40 (Continued)	811.9	$-0.038 \pm 0.010$	$0.001 \pm 0.011$	b
	829.8	$0.504 \pm 0.064$	$-0.011 \pm 0.075$	d
	1009.2	$-0.090 \pm 0.078$	$0.012 \pm 0.096$	$0.059 \leq \delta \leq 0.151$
	1114.6	$-0.014 \pm 0.037$	$0.012 \pm 0.043$	$-0.127 \leq \delta \leq -0.049$
	1561.7	$0.020 \pm 0.724$	$-0.104 \pm 0.806$	g

<sup>a</sup> The weak  $\gamma$ -ray feedings from higher-lying states have been ignored in determining these mixing ratios.

<sup>b</sup> The  $\gamma$ -ray feedings from higher-lying states for these cases could not be ignored, hence, no value for the mixing ratio could be determined.

<sup>c</sup> The  $\gamma$ -ray feeding from the higher-lying  $0^+$  state at 1450.8 keV has been taken into account in these cases, hence, the corrected values for  $A_2^*$  and  $A_4^*$  and the corresponding range of the mixing ratio.

<sup>d</sup> The  $4^+$   $\delta$  ellipse lies outside the ranges of  $A_2^*$  and  $A_4^*$  for these cases.

<sup>e</sup> See the text for discussion of the pure multipole order.

<sup>f</sup> This value is unlikely; see text for explanation.

<sup>g</sup> The errors on  $A_2^*$  and  $A_4^*$  for these cases are too large to allow a determination of the mixing ratio.

<sup>h</sup> The  $\gamma$ -ray angular distribution for this case has anomalously become isotropic for possible reasons discussed in the text. The possible ranges of  $\delta$  given may therefore not be valid.

mental range of the  $A_2^*$  and  $A_4^*$  coefficients. It should also be noted that the 0.1% confidence limit here is at reduced  $\chi^2 = 2.27$  provided that the assigned uncertainties are "accurate." Finally, the uncertainties of the  $A_2^*$  and  $A_4^*$  coefficients were almost independent of the errors assigned to the individual data points and were therefore essentially determined by the data-point scatter about the fit. Because the angular distributions usually included 20 points, these uncertainties can be assumed to be approximately 1 standard deviation errors.

The measured mixing ratios are presented in Table VI. The ranges were determined from the 1 standard deviation errors in the  $A_2^*$  and  $A_4^*$  coefficients. (In virtually every case, the appropriate  $\delta$  ellipse passed through a sufficient portion of the  $A_2^*$  and  $A_4^*$  range to allow the quoted range of mixing ratio to reflect the experimental error.) When more than one measurement of  $\delta$  existed, an average of the several values was made. More weight was given to those cases with smaller errors in the  $A_2^*$  and  $A_4^*$  coefficients. The final averaged values suggested for the mixing ratios of the various  $^{56}\text{Co}$   $\gamma$  rays measured in the present work are given in Table VIII of Sec. V.

#### D. Total Absolute Cross Sections at $E_p = 7.30$ MeV

A 7.30-MeV proton beam from the MSU cyclotron was used to bombard the  $^{56}\text{Fe}$  foil, which was placed at  $55^\circ$  with respect to the beam direction. The 2.5%-efficient Ge(Li) detector was positioned

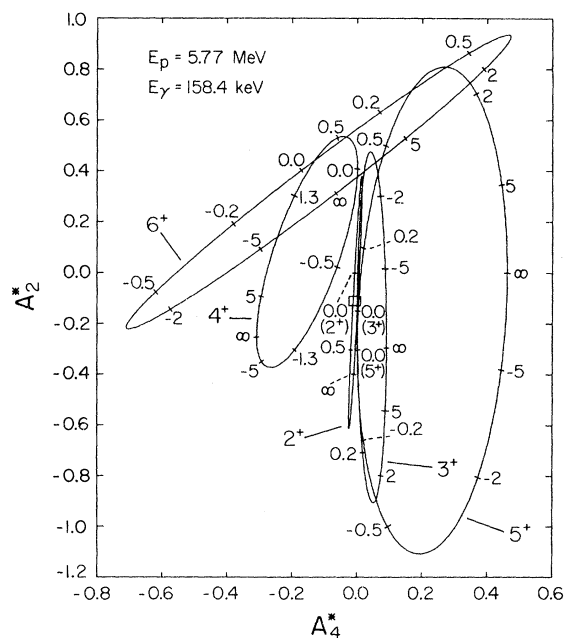


FIG. 12. Representative plot of MANDY predictions for the  $A_2^*$  and  $A_4^*$  coefficients as a function of  $\gamma$ -ray mixing ratio  $\delta$ . (Definitions are presented in the text.) This plot is for the case of the 158.4-keV  $\gamma$  ray at  $E_p = 5.77$  MeV. A spin of 4 for the final state was used; the spins and parities of the initial state label their appropriate  $\delta$  ellipses. The  $1^+$  "ellipse" (not shown) both here and for all cases is a short straight line having  $A_4^* = 0.0$  and passing through  $A_2^* = 0.0$ . The  $0^+$  "ellipse" is the single point  $A_2^* = 0.0$ ,  $A_4^* = 0.0$ . Representative values of  $\delta$  are labeled. The experimental  $A_2^*$  and  $A_4^*$  coefficients including uncertainties are shown as a rectangle in approximately the center of the plot.

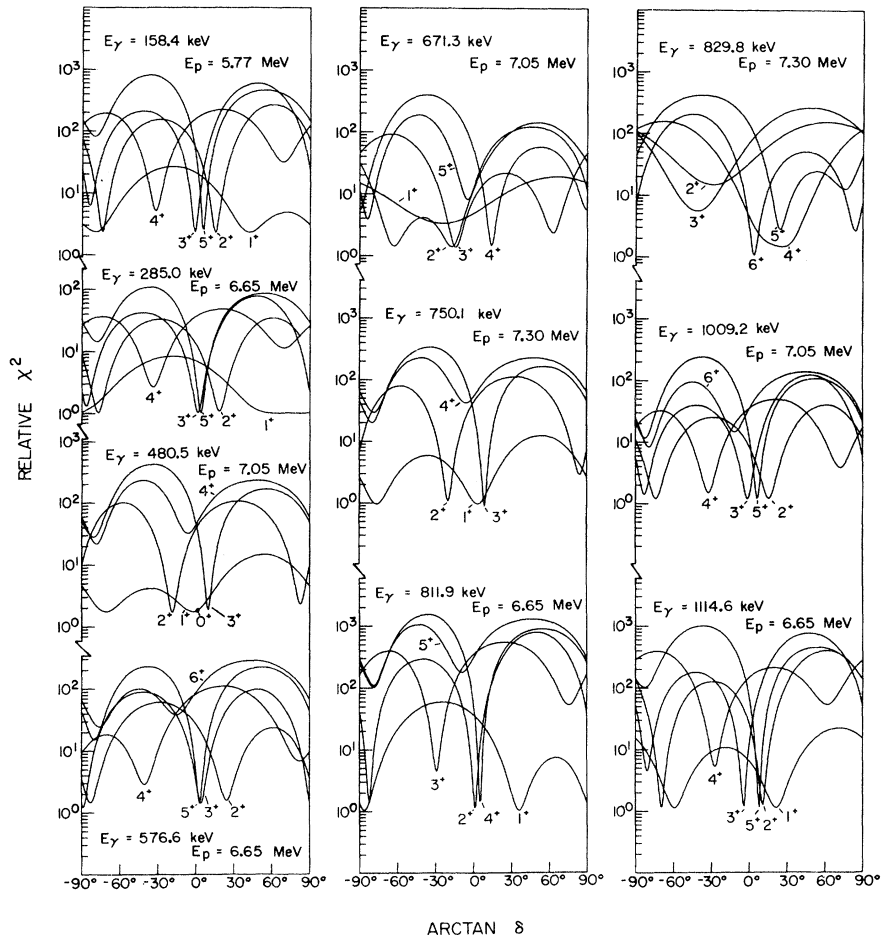


FIG. 13. Representative relative  $\chi^2$  versus  $\arctan\delta$  plots for angular distributions of each of the  $^{56}\text{Co}$   $\gamma$  rays.  $J^\pi$  values for the initial states label each curve. The  $J$  value assumed for the final state was that previously assigned in this work. For the 480.5-keV  $\gamma$  ray the  $0^+$  "curve" is a single point at  $\arctan\delta = 0^\circ$ .

with its face 12.7 cm from the center of the target and at  $90^\circ$  to the beam. Dead time and amplifier pileup corrections were made as described for the excitation function measurements. The charge was collected and integrated in a shielded 200-cm-long, 8.3-cm-diam piece of lead-lined aluminum beam pipe. The  $0.90 \pm 0.09$ -mg/cm<sup>2</sup> target thickness was determined by measuring the energy loss of 5.48-MeV  $\alpha$  particles from an  $^{241}\text{Am}$  source. The target was placed 15 cm in front of the Faraday cup described above. Since the rms angle for beam scattering from the target is approximately  $1^\circ$ , all of the charge should have entered the charge-collecting section of the beam pipe. The absolute normalization of the counting efficiency curve was determined for the geometry used by counting  $^{57}\text{Co}$ ,  $^{137}\text{Cs}$ ,  $^{54}\text{Mn}$ , and  $^{60}\text{Co}$  intensity standards. The precision quoted for the standards was  $\pm 5\%$ .<sup>61</sup> Care was taken to place the standards as close as possible to the position of the beam spot on target. Cor-

rections for  $\gamma$ -ray angular distribution effects were included in the analyses; however, corrections for internal conversion and target self-absorption were neglected since these were expected to be small in comparison to experimental errors.

Major experimental uncertainties lie in the target thickness (estimated uncertain by  $\pm 10\%$ , including nonuniformities), the integrated charge (estimated at  $\pm 5\%$ ), the absolute normalization for the efficiency curve (approximately  $\pm 10\%$ , including uncertainty in source positioning), and the  $\gamma$ -ray peak areas ( $\pm 2$  to  $\pm 7\%$ ). The total error associated with the measurement is then approximately  $\pm 15\%$ .

The neutron feeding to each state was determined from the absolute  $\gamma$ -ray intensities as described in the excitation function work. The  $(p, n)$  cross sections were finally calculated using these neutron feedings. The results are listed in Table VII. Included in the table are the total absolute cross-section predictions of MANDY for  $E_p = 7.30$

TABLE VII.  $^{56}\text{Fe}(p, n)^{56}\text{Co}$  total cross sections at  $E_p = 7.30$  MeV.

Excitation energy (keV)	Experimental		Theoretical <sup>a</sup>		
	$\sigma$ (mb)	$\sigma_{\text{rel}}^b$	$\sigma$ (mb)	$\sigma_{\text{rel}}^b$	$J^\pi$
158.4 ± 0.1	50.7 ± 7.8	≡1.000	81.3	≡1.000	3 <sup>+</sup>
576.6 ± 0.1	8.9 ± 1.2	0.176	14.4	0.177	5 <sup>+</sup>
829.7 ± 0.1	18.5 ± 2.6	0.365	23.1	0.284	4 <sup>+</sup>
970.3 ± 0.1	46.9 ± 6.7	0.925	66.4	0.816	2 <sup>+</sup>
1009.2 ± 0.1	6.2 ± 0.9	0.122	8.8	0.108	5 <sup>+</sup>
1114.6 ± 0.1	23.8 ± 3.3	0.469	38.1	0.469	3 <sup>+</sup>
1450.8 ± 0.1	23.9 ± 3.3	0.471	17.5	0.215	0 <sup>+</sup>
1720.3 ± 0.1	14.0 ± 2.0	0.276	17.3	0.213	1 <sup>+</sup>

<sup>a</sup> Theoretical total cross sections are only presented for those values of  $J^\pi$  suggested by this work.

<sup>b</sup>  $\sigma_{\text{rel}} = \sigma / \sigma_{158.4}$ .

MeV, as well as a comparison of the relative cross sections normalized to that of the 158.4-keV first excited state. The theoretical total cross sections listed are for the  $J^\pi$  values suggested by this work. Because of the fluctuations in the excitation functions, the total cross sections measured here are expected to deviate randomly from the theoretically predicted values. However, except for the cross section to the 1450.8-keV state, which appears to have a maximum in this energy region (see Fig. 8), the measured total cross sections are on the average 30% below the theoretically predicted values. Accurate quantitative comparison cannot be made between these measurements and the excitation function data because the experiments were performed with different accelerators, and the beam energy of the MSU cyclotron has not been calibrated precisely at these low energies. The nominal beam energies of the two accelerators are expected to be consistent within a few kilovolts, however.

Four possible explanations can be suggested for the 30% discrepancy. First, an unknown systematic error could have caused the experiment to yield incorrect results. Second, the transmission coefficients used in the MANDY calculations, although good enough to yield reasonable  $\gamma$ -ray angular distribution and relative cross-section predictions, could yield inaccurate absolute cross sections. Third, the calculations included all open neutron exit channels but were restricted to 14 proton exit channels. The open proton channels used corresponded to a maximum excitation in  $^{56}\text{Fe}$  of about 4 MeV. With 7.28 MeV of incident proton energy, an excitation of about 7.15 MeV is expected. Thus, a multitude of open proton channels in this additional 3-MeV excitation range were not taken into account. Although inclusion

of these additional channels would reduce the predicted cross sections, the effect could not be large since, as mentioned earlier, the limited phase space available to such low-energy particles and the 5.39-MeV Coulomb barrier both act to reduce the transmission coefficients considerably. The absolute cross-section predictions presented in Table VII, using 14 open proton exit channels, were on the average 7% smaller than the results of a similar calculation using 8 open proton exit channels. Finally, the Moldauer level-width fluctuation correction<sup>92</sup> was not included in this calculation. This correction would reduce slightly the magnitude of the total absolute cross sections but would have a pronounced effect only at much lower bombarding energies.

#### IV. DISCUSSION OF INDIVIDUAL LEVELS

Excluding the ground and first excited states, the spin assignments resulting from the present work are based upon the following criteria. First, the comparisons of the cross-section ratios with the theoretical predictions of MANDY are used to determine possible spin assignments. (In some cases these choices are unambiguous.) Second, these possibilities are further narrowed using the analyses of the  $\gamma$ -ray angular distributions. Finally, in the cases where two or more spin possibilities remain,  $\gamma$ -ray multiplicities determined from previous internal-conversion electron and lifetime measurements are compared with those multiplicities that are required to be consistent with the various spin choices and the  $\gamma$ -ray angular distribution data. It should be noted that for all firm spin assignments made here the first and second criteria stated above are met. Also, other possible spin values, although eliminated by the cross-section ratio comparisons, have been included in the relative  $\chi^2$  plots in Fig. 13 to emphasize the difficulty of making spin assignments to states of  $^{56}\text{Co}$  solely on the basis of  $\gamma$ -ray angular distributions. Finally, throughout the following discussions it is assumed that only even-parity states exist below 1.8 MeV of excitation in  $^{56}\text{Co}$  as discussed in Sec. III A. This assumption is necessary because the experimental uncertainties are greater than the sensitivities required to make parity assignments from either the cross-section ratios or the  $\gamma$ -ray angular distributions.

##### A. Ground State, $J^\pi = 4^+$

The ground-state spin is not directly measured in this experiment but is important since it in part determines the  $A_2^*$  and  $A_4^*$  coefficients for the  $\gamma$ -ray angular distributions of the five ground-state

transitions. Fortunately, the ground-state  $J^\pi$  has been previously determined to be  $4^+$  by such diverse methods as  $\gamma$ - $\gamma$  angular correlation,<sup>1,3</sup> hyperfine structure in paramagnetic resonance,<sup>63</sup> several different particle-transfer and charge-exchange reactions (references listed earlier), and inference from the  $\log ft$  data for its decay to states in  $^{56}\text{Fe}$ .<sup>64</sup> It should be noted that consistencies in the present work support this assignment.

B.  $E_x = 158.4$  keV,  $3^+$

The plot in Fig. 13 for the ground-state transition from this state shows pronounced minima in relative  $\chi^2$  for the  $J^\pi$  possibilities of  $1^+$ ,  $2^+$ ,  $3^+$ , and  $5^+$ . A less pronounced minimum is exhibited for  $J^\pi = 4^+$  suggesting that this choice is less likely. A careful study of Fig. 12 shows that  $J^\pi = 6^+$  can be eliminated. Since the angular distribution of the 158.4-keV  $\gamma$  ray is not isotropic (see Fig. 11 and Table VI),  $J^\pi = 0^+$  can also be eliminated.

Previous internal-conversion electron measurements by Menti,<sup>65</sup> Jenkins and Meyerhof,<sup>2</sup> and Ohnuma, Hashimoto, and Tomita,<sup>3</sup> as well as lifetime measurements by Wells *et al.*,<sup>1</sup> have shown that the 158.4-keV transition is predominantly  $M1$  in character. This fact rules out the  $J^\pi = 1^+$  possibility, since either a 45%  $M3$  + 55%  $E4$  or 3%  $M3$  + 97%  $E4$  transition is required to be consistent with the two minima observed for  $J^\pi = 1^+$  in relative  $\chi^2$ . Similarly, the  $J^\pi = 2^+$  possibility is ruled out, since a 93.2%  $E2$  + 6.8%  $M3$  or 7.6%  $E2$  + 92.4%  $M3$  transition is required.

The  $J^\pi = 4^+$  and  $5^+$  possibilities can be eliminated by comparing the changes in the theoretically predicted cross section as a function of beam energy with the measured excitation function for this state. (See Fig. 8.) The experimental cross section changes at most by a factor of 2 from a beam energy of 5.77 to 7.30 MeV, while the change predicted by MANDY is a factor of 7.4 for  $J^\pi = 4^+$  and 6.0 for  $J^\pi = 5^+$ . The change predicted for  $J^\pi = 3^+$  is 1.4.

Thus,  $J^\pi = 3^+$  is the only value consistent with the known  $M1$  character of the 158.4-keV  $\gamma$  ray and with the results of the present experiments. From its angular distribution, an  $M1$  transition with a 0.003 to 0.16%  $E2$  admixture is indicated for the 158.4-keV  $\gamma$  ray. A mixing ratio  $-0.04 \leq \delta \leq -0.006$  (see Tables VI and VIII) is in excellent agreement with the value  $-0.045 \leq \delta \leq 0.014$  measured by Ohnuma *et al.*<sup>3</sup> and the value  $-0.33 \leq \delta \leq 0.00$  measured by Wells *et al.*,<sup>1</sup> both using  $\gamma$ - $\gamma$  angular correlations in the  $\epsilon$  decay of  $^{56}\text{Ni}$ .

The 158.4-keV  $\gamma$ -ray angular distribution reported by Menti<sup>65</sup> using the  $(p, n\gamma)$  reaction is in complete disagreement with the present experiment.

Menti's measurement of  $A_2^* = 0.258 \pm 0.027$  and  $A_4^* = -0.125 \pm 0.028$  at  $E_p = 5.8$  MeV is not consistent with our values of  $A_2^* = -0.110 \pm 0.018$  and  $A_4^* = -0.008 \pm 0.020$  at  $E_p = 5.77$  MeV. This was the only  $^{56}\text{Co}$   $\gamma$ -ray angular distribution reported by Menti. The internal consistency of our data and their agreement with other types of experiments suggest that the coefficients reported by Menti are in error.

C.  $E_x = 576.6$  keV,  $5^+$

The cross-section ratio plot in Fig. 9 shows an unambiguous choice of  $J^\pi = 5^+$  for this state. A pronounced minimum in relative  $\chi^2$  is observed for  $J^\pi = 5^+$  in the plot of Fig. 13 for the ground-state transition from this state. An  $M1$  transition with 0.16 to 0.5%  $E2$  admixture is indicated for this  $\gamma$  ray.

D.  $E_x = 829.7$  keV,  $4^+$

The cross-section ratio plot in Fig. 9 shows an unambiguous choice of  $J^\pi = 4^+$  for this state. Both  $\gamma$ -ray branches from this state have analyzable angular distributions. It should be noted that for all of the  $\gamma$ -ray angular distribution measurements in which the 829.7-keV state was excited, it was also fed from above by a weak 285.0-keV  $\gamma$  transition. The feeding intensity was never more than 17% of the total intensity from the 829.7-keV state and was found to cause changes in the  $A_2^*$  and  $A_4^*$  coefficients that were much less than the quoted errors. The feeding was therefore ignored in the following analysis.

The angular distribution of the 671.3-keV  $\gamma$  yields a pronounced minimum in relative  $\chi^2$  for  $J^\pi = 4^+$  in the plot of Fig. 13. A predominantly  $M1$  transition with 4.6 to 7.3%  $E2$  admixture is indicated for this  $\gamma$  ray.

The 829.8-keV  $\gamma$ -ray angular distribution shows somewhat anomalous behavior. The experimental  $A_2^*$  for every beam energy is consistently large and positive. Only large error bars in three cases allow intersection with the  $4^+$   $\delta$  ellipse. (The  $\delta$  ellipses for this case are very similar to those of Fig. 12.) The  $\delta$  ellipse is approached more closely as the beam energy increases, however. A possible explanation is that since the peak is very weak, systematic errors are allowed to enter during the critical background subtraction process. The background exhibits a large anisotropy with  $A_2^* = 0.26 \pm 0.01$  and  $A_4^* = -0.07 \pm 0.01$  in this region of the  $\gamma$ -ray energy spectrum. A diffuse minimum is observed in relative  $\chi^2$  for  $J^\pi = 4^+$  in the plot of Fig. 13. A predominantly  $M1$  transition with 2.2 to 33%  $E2$  admixture is possible for this  $\gamma$  ray.

E.  $E_x = 970.3$  keV,  $2^+$ 

The choice of  $J^\pi$  from the cross-section ratio plot in Fig. 9 for this state is ambiguous, since the points scatter equally as well about the  $1^+$ ,  $2^+$ , and, less likely,  $3^+$  theoretical lines. A  $\gamma$ -ray transition of 811.9 keV to the  $3^+$  first excited state is the only  $\gamma$  ray observed to deexcite this state. The depths of the minima in relative  $\chi^2$  in the plot of Fig. 13 for the angular distribution of this  $\gamma$  ray, eliminate the  $J^\pi = 3^+$  possibility but leave both the  $1^+$  and  $2^+$  choices. Internal-conversion electron measurements by Ohnuma *et al.*<sup>3</sup> have shown that the 811.9-keV  $\gamma$  ray is predominantly  $M1$ . This fact rules out the  $J^\pi = 1^+$  possibility, since either a 65%  $E2 + 35\%$   $M3$  or 0.5%  $E2 + 99.5\%$   $M3$  transition would be required.

Thus,  $J^\pi = 2^+$  is the only value consistent with the known  $M1$  character of the 811.9-keV  $\gamma$  ray and with the results of the present experiments. Two pronounced minima in relative  $\chi^2$  are observed for  $J^\pi = 2^+$ . One minimum requires a 1.7%  $M1 + 98.3\%$   $E2$  transition. Since this multipole mixing is inconsistent with the  $M1$  character of this  $\gamma$  ray, it can be discarded. The other minimum requires an  $M1$  transition with 0.01 to 0.16%  $E2$  admixture. A mixing ratio  $0.01 \leq \delta \leq 0.04$  (see Tables VI and VIII) is in excellent agreement with the value  $-0.025 \leq \delta \leq 0.12$  measured by Ohnuma *et al.*<sup>3</sup> using  $\gamma$ - $\gamma$  angular correlations in the  $\epsilon$  decay of  $^{56}\text{Ni}$ .

F.  $E_x = 1009.2$  keV,  $5^+$ 

The cross-section ratio plot in Fig. 9 shows an unambiguous choice of  $J^\pi = 5^+$  for this state. Although two  $\gamma$ -ray branches are observed for this state, only the 1009.2-keV ground-state transition is strong enough to allow an angular distribution analysis. A pronounced minimum in relative  $\chi^2$  in the plot of Fig. 13 is observed for the  $5^+$  choice. An  $M1$  transition with a 0.36 to 2.2%  $E2$  admixture is indicated for the 1009.2-keV  $\gamma$  ray.

G.  $E_x = 1114.6$  keV,  $3^+$ 

The cross-section ratios for this state (Fig. 9) are scattered about the  $J^\pi = 3^+$  theoretical line with other possible, but less likely, choices being  $0^+$  or  $1^+$ . The  $2^+$  choice seems very unlikely, since only two data points even come close to its theoretical line. Three  $\gamma$ -ray branches are observed for this state with two, the 285.0- and 1114.6-keV  $\gamma$  rays, having analyzable angular distributions. The asymmetric 285.0-keV  $\gamma$ -ray angular distributions shown in Fig. 11 rule out  $J^\pi = 0^+$ . The  $J^\pi = 1^+$  possibility cannot be ruled out on the basis of the  $\gamma$ -ray angular distributions, however, since

pronounced minima in relative  $\chi^2$  in the plots of Fig. 13, are observed for  $J^\pi = 1^+$  for both  $\gamma$  rays.

This level does not deexcite as would be expected for a  $1^+$  state. For this choice the lowest multipole order possible for the  $\gamma$ -ray branches to the two  $4^+$  states fed would be  $M3$ . Assuming the  $B(M3)$ 's of these transitions to be comparable in magnitude, the energy dependence of the transition probability alone would require the 1114.6-keV transition to be  $10^4$  times as intense as the 285.0-keV transition. The measured value is only 8.5. Also, the 956.1-keV  $\gamma$  branch to the first excited  $3^+$  state would be an  $E2$  transition. The lifetime against such an  $E2$  decay is  $10^7$  (Weisskopf estimate) times as small as that for an  $M3$  decay. The fact that this branch is so weak (5% of the decays) would be inexplicable without a remarkable accidental cancellation of matrix elements.

Finally, additional but weaker arguments are that a  $J^\pi = 1^+$  assignment would open up the possibility of feeding from the decay of  $^{56}\text{Ni}$ , the possibility of  $\gamma$ -ray feeding from both the higher-lying  $0^+$  and  $1^+$  states at 1450.8 and 1720.3 keV, respectively, and the possibility of  $\gamma$ -ray decay to the lower-lying  $2^+$  state at 970.3 keV. None of these phenomena are observed. A  $J^\pi = 1^+$  assignment is therefore highly unlikely and only  $J^\pi = 3^+$  remains.

Pronounced minima in relative  $\chi^2$  in the plot of Fig. 13 for  $J^\pi = 3^+$  are observed for both the 285.0- and 1114.6-keV  $\gamma$  rays. An  $M1$  transition with a 0.0 to 0.6%  $E2$  admixture is indicated for the 285.0-keV  $\gamma$  ray, and an  $M1$  transition with a 0.36 to 1.2%  $E2$  admixture is indicated for the 1114.6-keV  $\gamma$  ray.

H.  $E_x = 1450.8$  keV,  $0^+$ 

The cross-section ratios for this state (Fig. 9) are scattered about the  $J^\pi = 0^+$  theoretical line with other choices of  $3^+$  or  $4^+$  seemingly possible. The  $1^+$  and  $2^+$  choices seem very unlikely, since only one data point even comes close to their theoretical lines. A  $\gamma$ -ray transition of 480.5 keV to the  $2^+$  fourth excited state at 970.3 keV is the only  $\gamma$  ray observed to deexcite this state. The angular distribution for this 480.5-keV  $\gamma$  ray is isotropic (see Fig. 11). The isotropy is a necessary (although nonsufficient) condition for a spin-zero assignment. A pronounced minimum in relative  $\chi^2$  in the plot of Fig. 13 is not observed for  $J^\pi = 4^+$  and clearly eliminates this possibility. However, a pronounced minimum is observed for  $J^\pi = 3^+$ . Conversion-electron measurements by Jenkins and Meyerhof,<sup>2</sup> and by Ohnuma *et al.*,<sup>3</sup> as well as lifetime measurements by Wells *et al.*,<sup>1</sup> have shown that this transition is  $E2$ . The necessary mixing ratio for the  $J^\pi = 3^+$  possibility, however,



is  $0.16 \leq \delta \leq 0.20$ , giving at most a 96.2%  $M1 + 3.8\%$   $E2$  transition. A  $J^\pi = 0^+$  assignment on the other hand requires the 480.5-keV  $\gamma$  transition to be pure  $E2$ . Thus,  $J^\pi = 0^+$  is the only value consistent with the known  $E2$  character of the 480.5-keV  $\gamma$  ray and with the results of the present experiments.

Because of the abnormally long half-life of this state ( $1.6 \pm 0.1$  nsec),<sup>1</sup> a supplementary experiment was performed to investigate possible nuclear hyperfine interaction effects caused by the expected large internal magnetic field ( $\approx 333$  kOe)<sup>66</sup> in the vicinity of the target nuclei in the  $^{56}\text{Fe}$  target. A proton beam of 7.52 MeV was used to bombard a 0.02-mg/cm<sup>2</sup> stainless-steel target. In this stainless-steel target the magnetic field in the vicinity of the nuclei is minimal, thus, angular distribution "washout" due to precession of the magnetic moment should be greatly reduced. Partial angular distributions (10 data points) clearly showed an isotropic distribution for the 480.5-keV  $\gamma$  ray ( $A_2^* = 0.01 \pm 0.02$  and  $A_4^* = 0.00 \pm 0.03$ ). Other  $^{56}\text{Co}$   $\gamma$  rays preserved their previous behavior observed in the  $^{56}\text{Fe}$  foil target (e.g., the 269.5-keV transition had  $A_2^* = -0.30 \pm 0.10$  and  $A_4^* = 0.01 \pm 0.13$ ).

As discussed earlier,  $J^\pi$  assignments of  $1^-$  and  $2^+$  have been suggested for this state. These suggestions are incompatible with the measured cross-section ratios. The odd-parity possibilities, which are not shown on the plot of Fig. 9, require, for example, cross-section ratios of 0.543 for  $J^\pi = 1^-$  and 0.573 for  $J^\pi = 2^-$  at  $E_p = 7.68$  MeV. These values are very close to the  $J^\pi = 1^+$  and  $2^+$  theoretical points and are about 2.5 times the average of the two closest measured ratios, 0.198. The  $J^\pi = 0^+$  assignment suggested in this work was essentially eliminated in the  $\gamma$ - $\gamma$  angular correlation analyses by Wells *et al.*<sup>1</sup> and Ohnuma *et al.*<sup>3</sup> (using the  $\epsilon$  decay of  $^{56}\text{Ni}$ ) on the basis of their error assignments to the angular correlation coefficients. An increase to 2 standard deviations in their reported errors would have resulted in compatibility with the  $J^\pi = 0^+$  assignment.<sup>67</sup>

The additional suggestion that two states exist in this region of excitation with  $J^\pi = 0^+$  and  $1^-$  is also incompatible with the present work. From the  $\gamma$ -ray singles and  $\gamma$ - $\gamma$  coincidences measured using the  $^{56}\text{Ni}$  decay, no evidence could be found for  $\gamma$  rays deexciting a second state near 1451 keV. The FWHM for both the 269.5- and 480.5-keV peaks (exciting and deexciting the 1450.8-keV state, respectively) as determined by SAMPO were predicted to within 0.9 and 0.4%, respectively, using a least-squares linear fit to the FWHM values and energies of the seven other most prominent peaks (other than the 511.0-keV annihilation radiation peak) in the spectrum of Fig. 1. Assuming doublet

members with approximately the same intensity, an increase in the FWHM value of 5% corresponds to a centroid difference of only 0.02 keV. Similarly, from  $\gamma$ -ray singles and  $\gamma$ - $\gamma$  coincidences measured using the  $^{56}\text{Fe}(p, n\gamma)^{56}\text{Co}$  reaction, no evidence could be found for  $\gamma$  rays deexciting an additional state in this region. Here, as opposed to the  $\beta$  decay, all existing states are expected to be excited, although the high-spin states are expected to be excited only weakly. Since the additional state was suggested to have  $J^\pi = 1^-$ , a large predicted cross section should produce a reasonably large  $\gamma$ -ray peak or peaks. As before, the FWHM for both the 269.5- and 480.5-keV peaks (from a randomly chosen excitation function spectrum) were predicted to within 3.2 and 2.2%, respectively. If the 1450.8-keV state were really a very close-lying doublet with both members deexciting via a 480.5-keV  $\gamma$  ray, the cross-section ratios should be  $\approx 3.5$  times the measured values. In view of the internal consistency of the present data, this value is a much larger inconsistency than would be expected.

Finally, the energies of the 269.5- and 480.5-keV  $\gamma$  rays were measured independently (using different energy standards) to be the same within the experimental errors of  $\pm 0.1$  keV using both the  $^{56}\text{Ni}$  decay and the  $^{56}\text{Fe}(p, n\gamma)^{56}\text{Co}$  reaction. Thus, it is concluded that there is strong evidence that only one state exists in  $^{56}\text{Co}$  in the region of 1451 keV of excitation, namely, at 1450.8 keV, and the state has  $J^\pi = 0^+$ .

#### I. $E_x = 1720.3$ keV, $1^+$

The cross-section ratios for this state show a scatter of points about the  $J^\pi = 1^+$  and  $2^+$  theoretical lines and in close proximity to the  $0^+$  and  $3^+$  lines. Three  $\gamma$ -ray branches are observed for this state with two, the 269.5- and 750.1-keV  $\gamma$  rays having analyzable angular distributions. The  $J^\pi = 0^+$  possibility is eliminated by the anisotropic distribution of the 269.5-keV  $\gamma$  (see Fig. 11). The relative  $\chi^2$  plot for the 750.1-keV  $\gamma$  ray sheds little light on possible  $J^\pi$  assignments since all the remaining choices have pronounced minima.

The 269.5-keV  $\gamma$ -ray angular distribution is more illuminating, however. Since this transition goes to a spin-zero state, the  $\delta = 0$  requirement yields theoretical angular distribution coefficients that are unique (i.e., it must be a pure multipole transition). The coefficients predicted by MANDY at  $E_p = 7.30$  MeV for  $J^\pi = 1^+$  are  $A_2^* = -0.218$  and  $A_4^* = 0.000$ , for  $J^\pi = 2^+$  are  $A_2^* = 0.517$  and  $A_4^* = -0.302$ , and for  $J^\pi = 3^+$  are  $A_2^* = 0.842$  and  $A_4^* = 0.136$ . The measured values of  $A_2^* = -0.296 \pm 0.023$  and  $A_4^* = 0.030 \pm 0.031$  at  $E_p = 7.30$  MeV are compatible only

with  $J^\pi = 1^+$ , since  $J^\pi = 2^+$  and  $3^+$  require large positive values of  $A_2^*$ . The measured value of  $A_2^*$  is, however, still almost 4 standard deviations more negative than the predicted value. Najam *et al.*<sup>68</sup> observed this same type of behavior for a  $1^+$  state in a  $^{66}\text{Zn}(p, n\gamma)^{66}\text{Ga}$  experiment at a proton beam energy of approximately 6.50 MeV. They attribute this behavior to a direct reaction component for the  $(p, n\gamma)$  reaction.

To investigate this somewhat anomalous behavior further, an additional  $\gamma$ -ray angular-distribution measurement was made with the beam energy increased by just 100 keV (from 7.30 to 7.40 MeV). The angular distribution for the 269.5-keV  $\gamma$  ray obtained at the new energy was, very surprisingly, essentially isotropic, with  $A_2^* = -0.018 \pm 0.025$  and  $A_4^* = 0.006 \pm 0.029$ . The angular distributions for all the other  $\gamma$  rays, except the 750.1-keV  $\gamma$  ray which had also become isotropic, remained virtually unchanged (see Table VI). The following possible explanation for this strange behavior supports the  $J^\pi = 1^+$  assignment.

Anisotropic  $\gamma$ -ray angular distributions result from alignment of the excited residual nuclei with respect to the beam direction. The addition of angular momentum from the incident proton causes the original alignment of the compound nucleus, which then, after neutron decay, results in alignment of the excited residual nucleus. Assuming  $s$ -wave exit neutrons,  $l_n = 0$  (expected near threshold), a final state with spin 1 can only be reached with  $s$ -,  $p$ -, and  $d$ -wave protons,  $l_p = 0, 1,$  and  $2$ , since the  $^{56}\text{Fe}$  target nuclei have  $J^\pi = 0^+$ . The parity selection rule,  $\pi_f = \pi_i$  for  $l_p + l_n = \text{even}$ , further requires  $l_p = \text{even}$  only, since  $\pi_f = \pi_i = +1$  and  $l_n = 0$ . This restriction eliminates the participation of  $p$ -wave protons. Thus, the final state of  $J^\pi = 1^+$  can only be reached with  $s$ -wave protons going through  $\frac{1}{2}^+$  CN states and  $d$ -wave protons going through  $\frac{3}{2}^+$  CN states. No other combinations are allowed. States of residual nuclei reached with  $s$ -wave entrance protons and  $s$ -wave exit neutrons through  $\frac{1}{2}^+$  CN states can have no alignment since the proton imparts no orbital angular momentum to the compound nucleus and the spin of the neutron can be oriented in any direction. On the other hand, states of residual nuclei reached through  $\frac{3}{2}^+$  CN states created by  $d$ -wave entrance protons have some alignment. The exit neutron in this case can "wash out" the alignment but cannot destroy it. Resulting  $\gamma$ -ray angular distributions in the former case must be isotropic from the lack of nuclear alignment but in the latter case can be anisotropic. Because of the extremely restricted number of possibilities, a dominance in the compound nucleus (in either cross section or density of states) of one spin over the other can greatly affect the mag-

nitude of the subsequent  $\gamma$ -ray anisotropy. MANDY predicts a maximum possible value of  $A_2^* = -0.5$  for the case of only  $\frac{3}{2}^+$  states in the compound nucleus and  $A_2^* = 0.0$  for the case of only  $\frac{1}{2}^+$  states. This behavior is restricted to spin-1 states, since residual states of spin greater than 1 can always be reached by more than one pathway in which nuclear alignment is preserved, even if only one type of spin state is available in the compound system.

Thus,  $J^\pi = 1^+$  for the 1720.3-keV state is the only value consistent with the results of these experiments and with the above discussion. The 269.5-keV  $\gamma$  ray is thus pure  $M1$  which is consistent with the internal-conversion electron measurements by Jenkins and Meyerhof<sup>2</sup> and Ohnuma *et al.*<sup>3</sup> A mixing ratio of  $-0.04 \leq \delta \leq 0.25$  or  $-23 \leq \delta \leq -2.9$  is indicated for the 750.1-keV  $\gamma$  ray. The former value (i.e., an  $M1$  transition with a 0.0 to 5.9%  $E2$  admixture) is in reasonable agreement with the value  $-0.20 \leq \delta \leq 0.09$  measured by Ohnuma *et al.*<sup>3</sup> using  $\gamma$ - $\gamma$  angular correlation in the  $\epsilon$  decay of  $^{56}\text{Ni}$ . The mostly  $M1$  character is further supported by the internal-conversion electron measurements of Ohnuma *et al.*<sup>3</sup> The 1561.7-keV  $\gamma$  branch from this state to the  $3^+$  first excited state at 158.4 keV must be an  $E2$  transition by virtue of the angular-momentum change between these states.

#### J. Higher Excited States

Excitation functions and  $\gamma$ -ray angular distributions were not measured for any of the higher states. An increasingly complex  $\gamma$ -ray spectrum and rapidly decreasing detector efficiency with the increasing energies of newly encountered  $\gamma$  rays, would have made such measurements difficult. In addition, for the case of the  $\gamma$ -ray angular distributions, increasing beam energies resulted in higher levels of radiation from the lead beam stop. For these same reasons, no ground-state transitions were identified from these states in singles experiments.

Some comments can be made, however, about the  $\gamma$ -ray transitions from these states observed in the  $\gamma$ - $\gamma$  coincidence measurement at  $E_p = 8.36$  MeV. All of the spins suggested for these higher states by Schneider and Daehnick<sup>9</sup> (marked with asterisks in Fig. 6) from the  $^{58}\text{Ni}(d, \alpha)^{56}\text{Co}$  reaction are compatible with the assumption that there is at most a spin change of two between states connected by  $\gamma$ -ray transitions. This assumption suggests a spin 1 or 2 for the 2635.7-keV state by virtue of its 1184.9-keV  $\gamma$  transition to the  $0^+$  state at 1450.8 keV. No  $\gamma$ -ray transitions from the known states (see Ref. 9) at 2281 keV ( $7^+$ ) and 2371 keV ( $6^+, 5^+, 7^+$ ) were observed, presumably because the low-energy  $(p, n)$  cross sections to such high-

spin states are very small. Thus, the spin of the 2469.3-keV state must surely be 3, 4, or 5 by virtue of its observable 1892.7-keV  $\gamma$  transition to the  $5^+$  state at 576.6 keV. This 2469.3-keV state may be a  $4^+$  state predicted in this energy region by McGrory.<sup>28</sup> (See Fig. 14.) The lack of observed  $\gamma$ -ray transitions from the known state (see Ref. 9) at 2791 keV may result simply from a low cross section caused by low exit neutron energy and not from high spin. The existence of a state at 2289.8 keV suggested by DelVecchio *et al.*<sup>22</sup> is confirmed.

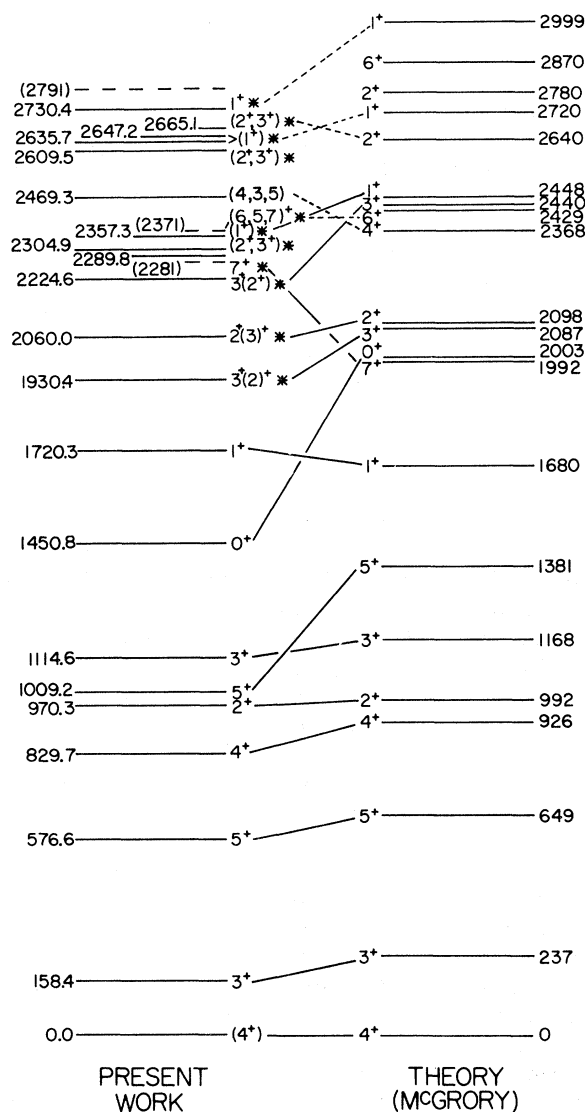


FIG. 14. Comparison of level spins, parities, and energies of the present experiment and from Ref. 9 (asterisked values), with the predictions of McGrory (Ref. 28). Dashed lines indicate tentative correlations. For excitations above 3 MeV, see Ref. 9.

### V. COMPARISONS WITH SHELL-MODEL CALCULATIONS FOR $^{56}\text{Co}$

The  $^{56}\text{Co}_{29}$  nucleus has one neutron outside and one proton hole inside an otherwise closed  $f_{7/2}$  shell. It thus lends itself quite nicely to shell-model calculations. McGrory<sup>28</sup> has recently performed a calculation in which  $^{56}\text{Co}$  was represented as a  $^{40}\text{Ca}$  core plus 14 or 15 nucleons in the  $f_{7/2}$  orbit and the remainder in the  $p_{3/2}$ ,  $f_{5/2}$ , or  $p_{1/2}$  orbits. He used single-particle energies which best reproduced the  $^{57}\text{Ni}$  spectrum and Kuo-Brown matrix elements for the effective two-body Hamiltonian. He then used the resulting  $^{56}\text{Co}$  wave functions to calculate the reduced transition probabilities,  $B(M1)$  and  $B(E2)$ , for all possible  $M1$  and  $E2$   $\gamma$ -ray decay channels for each of the predicted states. For the  $B(M1)$ 's the bare  $M1$  operator was used while for the  $B(E2)$ 's an effective charge of 0.5 was used.<sup>69</sup> These reduced transition probabilities are compared below with lifetime measurements by Wells *et al.*<sup>1</sup> and with the  $\gamma$ -ray multipole mixing ratios and branching ratios measured in this experiment. The same  $^{56}\text{Co}$  wave functions used in these calculations were quite successful in predicting strengths for deuteron pickup in a recent  $^{58}\text{Ni}(d, \alpha)^{56}\text{Co}$  experiment by Schneider and Daehnick.<sup>9</sup>

The spins, parities, and energies of the  $^{56}\text{Co}$  states predicted by McGrory and the corresponding experimental assignments of the present work are shown in Fig. 14. As can be seen, the agreement between theory and experiment is quite remarkable for the states below 1.8 MeV. Only the second  $5^+$  state and the  $0^+$  state are predicted too high in energy, and even these discrepancies are no more than 450 keV.

For the following discussion, the  $M1$  and  $E2$  transition probabilities,  $W(M1)$  and  $W(E2)$ , were calculated from the  $B(M1)$ 's and  $B(E2)$ 's computed by McGrory and presented in Table VIII, according to,<sup>70</sup>

$$W(M1) = 1.7588 \times 10^{13} E_\gamma^3 B(M1) \quad (\text{sec}^{-1})$$

and

$$W(E2) = 1.2258 \times 10^9 E_\gamma^5 B(E2) \quad (\text{sec}^{-1}),$$

where  $E_\gamma$  is the experimental  $\gamma$ -ray energy in MeV,  $B(M1)$  is the  $M1$  reduced transition probability in nuclear magnetons squared,  $\mu_N^2$ , and  $B(E2)$  is the  $E2$  reduced transition probability in  $e^2 \text{fm}^4$ . The predicted half-lives are then the reciprocals of the transition probabilities multiplied by  $\ln 2$ .

The calculated  $B(M1)$ 's range from 0.002 to  $2.5 \mu_N^2$  and the  $B(E2)$ 's range from 0.01 to  $100 e^2 \text{fm}^4$ . Thus, in light of the above equations, all  $\gamma$ -ray transitions with energies less than 1 MeV

TABLE VIII. Reduced transition probabilities,  $B(M1)$  and  $B(E2)$ , calculated by McGrory (see Ref. 28) and comparisons of the shell-model results with experimental  $\gamma$ -ray multipole mixing ratios,  $\delta$ , and  $\gamma$ -ray branching ratios from the  $^{56}\text{Fe}(p, n\gamma)^{56}\text{Co}$  reaction. The experimental transition energies were used when calculating the theoretical mixing and branching ratios (necessary formulas are presented in the text).

Transition $J_i^\pi \rightarrow J_f^\pi$	$E_\gamma$ <sup>a</sup> (keV)	$B(M1)$ ( $\mu_N^2$ )	$B(E2)$ ( $e^2 \text{fm}^4$ )	$\delta_{\text{th}}$ <sup>b</sup>	$\delta_{\text{exp}}$	Theoretical branching ratios <sup>c</sup> (%)	Experimental branching ratios <sup>c, d</sup> (%)
$3_1^+ \rightarrow 4_1^+$	158.4	1.60	74.1	+0.012	$-0.04 \leq \delta \leq -0.006$	100	100
$5_1^+ \rightarrow 3_1^+$	(418.2)	...	11.9	...		<0.05	<3
$5_1^+ \rightarrow 4_1^+$	576.6	0.350	34.6	+0.048	$0.04 \leq \delta \leq 0.07$	$\approx 100$	100
$4_2^+ \rightarrow 5_1^+$	(253.1)	0.0560	36.2	+0.054		21.3	<0.7
$4_2^+ \rightarrow 3_1^+$	671.3	0.0155	27.1	+0.234	$0.22 \leq \delta \leq 0.28$	66.5	$75.3 \pm 1.3$
$4_2^+ \rightarrow 4_1^+$	829.8	0.0020	16.2	-0.623	$(0.15 \leq \delta \leq 0.70)$ <sup>e</sup>	12.2	$24.7 \pm 1.3$
$2_1^+ \rightarrow 4_2^+$	(140.6)	...	0.0150	...		<0.05	<0.3
$2_1^+ \rightarrow 3_1^+$	811.9	0.704	8.48	+0.024	$0.01 \leq \delta \leq 0.04$	99.8	100
$2_1^+ \rightarrow 4_1^+$	(970.3)	...	9.77	...		0.2	<0.7
$5_2^+ \rightarrow 4_2^+$	(179.5)	0.609	77.1	+0.002		1.0	<2
$5_2^+ \rightarrow 5_1^+$	432.8	0.0536	0.0032	-0.001	f	1.2	$5.2 \pm 1.6$
$5_2^+ \rightarrow 3_1^+$	(850.8)	...	1.04	...		<0.05	<7
$5_2^+ \rightarrow 4_1^+$	1009.2	0.329	14.9	+0.057	$0.06 \leq \delta \leq 0.15$	97.7	$94.8 \pm 1.6$
$3_2^+ \rightarrow 5_2^+$	(105.4)	...	0.0116	...		<0.05	<0.3
$3_2^+ \rightarrow 2_1^+$	(144.3)	0.0168	3.83	+0.006		<0.05	<0.4
$3_2^+ \rightarrow 4_2^+$	285.0	0.792	59.0	+0.021	$-0.02 \leq \delta \leq 0.08$	24.6	$10.1 \pm 2.0$
$3_2^+ \rightarrow 5_1^+$	(538.0)	...	1.07	...		<0.05	<1
$3_2^+ \rightarrow 3_1^+$	956.1	0.0189	4.76	+0.127	f	22.5	$5.0 \pm 0.5$
$3_2^+ \rightarrow 4_1^+$	1114.6	0.0282	2.84	-0.093	$-0.11 \leq \delta \leq -0.06$	52.8	$84.9 \pm 1.9$
$0_1^+ \rightarrow 2_1^+$	480.5	...	10.4	$E2$	$E2$	100	100
$1_1^+ \rightarrow 0_1^+$	269.5	2.49	...	$M1$	$M1$	93.3	$36.4 \pm 5.3$
$1_1^+ \rightarrow 3_2^+$	(605.7)	...	1.42	...		<0.05	<3
$1_1^+ \rightarrow 2_1^+$	750.1	0.0068	0.438	+0.050	$-0.04 \leq \delta \leq 0.25$	5.5	$51.0 \pm 4.5$
$1_1^+ \rightarrow 3_1^+$	1561.7	...	0.967	...	f	1.2	$12.6 \pm 1.2$

<sup>a</sup>The energies shown in parentheses are possible transitions that have not been observed and whose magnitudes have been calculated using the measured level energies.

<sup>b</sup>The signs on  $\delta_{\text{th}}$  are the relative phases predicted by McGrory (Ref. 28).

<sup>c</sup>The branching ratio is the fraction of all  $\gamma$ -ray decays from the initial state proceeding by the transition considered.

<sup>d</sup>Branching ratios sum to 100 for all observed transitions from each state. Upper limits are shown for all unobserved transitions.

<sup>e</sup>This range of mixing ratio for the 829.8-keV  $\gamma$  ray is suspect as outlined in Sec. IVD.

<sup>f</sup>Because of poor peak statistics,  $\gamma$ -ray angular distributions for these transitions could not be measured.

are predicted to be predominantly  $M1$  except where  $M1$  transitions are not allowed by angular-momentum selection rules.

The above exception is the case for the  $0^+$  state at 1450.8 keV. If this state is  $0^+$ , no  $M1$  decay is possible and, in fact, only one  $E2$  channel, that to the  $2^+$  state at 970.3 keV, is open. McGrory's predicted half-life for this  $E2$  decay is 2.12 nsec (see Table IX). The only  $\gamma$ -ray decay observed from the 1450.8-keV state is that to the 970.3-keV state and it has a measured half-life of  $1.6 \pm 0.1$  nsec.<sup>1</sup> Even with the factor of 1.3 discrepancy (completely accountable by the somewhat arbitrary choice of 0.5 for the effective charge in the  $E2$  operator), this is remarkable agreement.

Only two additional states, at 158.4 and 970.3

keV, have previously measured lifetimes.<sup>1</sup> Upper limits for the half-lives of these states were set at 100 psec. The half-lives predicted by McGrory for these states are 10.9 and 0.105 psec, respectively. The very short half-life predicted for the 970.3-keV state accounts for the lack of an observable 970.3-keV  $E2$   $\gamma$ -ray branch to ground.

The predicted multipole mixing ratios presented in Table VIII were calculated from the equation

$$\delta^2 = \frac{W(E2)}{W(M1)}.$$

The predicted relative phases of  $\delta$  presented are those of McGrory. Except for the 829.8-keV transition whose anomalous behavior was discussed previously, the agreement between the theoretical

TABLE IX. Shell-model predictions by McGrory (see Ref. 28) of the half-lives of the first eight excited states of  $^{56}\text{Co}$ . Only observed transitions were included in these calculations. Internal-conversion effects were not included.

Excitation energy (keV)	$t_{1/2}^{\text{th}}$ <sup>a</sup> (psec)	$t_{1/2}^{\text{exp}}$ <sup>b</sup> (psec)
158.4	10.9	<100
576.6	0.586	
829.7	6.03	
970.3	0.105	<100
1009.2	0.115	
1114.6	0.529	
1450.8	$(2.12)10^3$	$(1.6 \pm 0.1)10^3$
1720.3	0.753	

<sup>a</sup> See Ref. 28.

<sup>b</sup> See Ref. 1.

and experimental mixing ratios is quite good. A particular case is the 671.3-keV transition from the first excited  $4^+$  state to the first excited  $3^+$  state. Here, compared to the  $E2$  admixtures of other predominantly  $M1$  transitions, a sizable  $E2$  strength of  $(5.9 \pm 1.4)\%$  is observed. The rather small  $B(M1)$  predicted for this transition causes enhancement of the theoretical  $E2$  strength (5.2%). Some quantitative agreement between theory and experiment is therefore indicated.

The theoretical and experimental  $\gamma$ -ray branching ratios are presented in Table VIII. In general, agreement is very good.

## VI. SUMMARY AND CONCLUSIONS

The  $\gamma$ -ray decays of the excited states of  $^{56}\text{Co}$  below 2.86 MeV of excitation have been studied via the electron-capture decay of  $^{56}\text{Ni}$  and the  $^{56}\text{Fe}(p, n\gamma)^{56}\text{Co}$  reaction. The adopted energies (in keV) of the six  $\gamma$  rays common to both studies are:  $158.4 \pm 0.1$ ,  $269.5 \pm 0.1$ ,  $480.5 \pm 0.1$ ,  $750.0 \pm 0.1$ ,  $811.9 \pm 0.1$ , and  $1561.9 \pm 0.2$ . The Ge(Li)-Ge(Li)  $\gamma$ - $\gamma$  coincidence technique used both on and off line was extremely useful in the placement of  $\gamma$  rays in the decay schemes. In particular, high-energy  $\gamma$  rays (greater than 1500 keV) could be separated in the in-beam spectra from otherwise overwhelming continuum backgrounds. In fact, the high background and diminishing detector efficiency for high-energy  $\gamma$  rays forced an end to the excitation function and  $\gamma$ -ray angular distribution measurements at about 2 MeV in  $^{56}\text{Co}$ . Since the statistical CN theory appears still valid at these excitations, these background problems are the only hindrance to a continuation of these measurements to higher excitations.

The combined use of cross-section ratios and

$\gamma$ -ray angular distributions proved very potent in determining unique spin assignments. The experimental errors of the  $\gamma$ -ray angular distributions and the experimental errors and fluctuations of the cross-section ratios were, however, greater than the sensitivities required to make parity determinations. Thus, it is necessary to assume all parities even based upon previous experimental results and shell-model considerations. Spin and parity assignments (in parentheses) were thus made for the following  $^{56}\text{Co}$  states (energies in keV): 158.4 ( $3^+$ ), 576.6 ( $5^+$ ), 829.7 ( $4^+$ ), 970.3 ( $2^+$ ), 1009.2 ( $5^+$ ), 1114.6 ( $3^+$ ), 1450.8 ( $0^+$ ), and 1720.3 ( $1^+$ ).

Comparisons of the experimental cross-section ratios and  $\gamma$ -ray angular distributions with the predictions of the statistical CN theory (via the code MANDY) showed remarkable agreement, with two notable exceptions. First, gross fluctuations, often 15% in magnitude and 40–100 keV in width (roughly 1–3 times the target thickness) were observed in the excitation function measurements. These fluctuations also manifested themselves in the cross-section ratios as scattering about the predicted values. A satisfying explanation for these gross fluctuations would be interesting and useful information. Second, otherwise anisotropic angular distributions (both predicted and observed) for two  $\gamma$ -ray decays of the 1720.3-keV  $1^+$  state became essentially isotropic when the beam energy was increased by 100 keV from 7.30 to 7.40 MeV. It would be interesting to know if the same behavior under similar conditions is observed for  $1^+$  states in other nuclei as would be predicted by the explanation offered in Sec. IVI. These two exceptions indicate partial breakdown in the statistical assumption of large numbers of overlapping CN states of random spin and parity.

No evidence was found in the present work for the existence of an additional level near the 1450.8-keV state. The cross-section ratio comparisons and the angular distributions of both the 480.5-keV  $\gamma$  deexciting the level and the 269.5-keV  $\gamma$  feeding it were uniquely compatible with a  $J^\pi = 0^+$  assignment to a single state.

The shell-model calculations of McGrory<sup>28</sup> are in excellent agreement with the measured level energies and spins particularly below 1.8 MeV. Also McGrory's calculations of the  $B(M1)$ 's and  $B(E2)$ 's agree, in general, with the  $\gamma$ -ray measurements reported here. Lifetime measurements for these states are needed for more direct comparisons with the predicted transition probabilities.

## ACKNOWLEDGMENTS

We are indebted to Dr. H. G. Blosser and H. Hilbert for their help in the operation of the MSU cyclo-

tron. We are also indebted to Eric Warren for his invaluable assistance in the operation of the Western Michigan University tandem Van de Graaff and PDP-15 computer. We wish to thank Dr. R. W. Goles, C. B. Morgan, and W. B. Chaffee for their aid in data collection and interpretation, and Dr.

B. H. Wildenthal for useful discussions concerning shell-model calculations provided by Dr. J. B. McGrory, to whom we extend a very special thanks. Mrs. Carol VanderMeer and Mrs. Peri-Anne Warstler aided us greatly in preparing the manuscript.

\*Present address: Department of Physics, Western Michigan University, Kalamazoo, Michigan 49001.

†Work supported in part by the U. S. National Science Foundation.

‡Alfred P. Sloan Fellow, 1972-1974.

§Work supported in part by the U. S. Atomic Energy Commission.

¶Work supported in part by the Research Corporation.

<sup>1</sup>D. O. Wells, S. L. Blatt, and W. E. Meyerhof, *Phys. Rev.* **130**, 1961 (1963).

<sup>2</sup>R. C. Jenkins and W. E. Meyerhof, *Nucl. Phys.* **58**, 417 (1964).

<sup>3</sup>H. Ohnuma, Y. Hashimoto, and I. Tomita, *Nucl. Phys.* **66**, 337 (1965).

<sup>4</sup>C. J. Piluso, D. O. Wells, and D. K. McDaniels, *Nucl. Phys.* **77**, 193 (1966).

<sup>5</sup>R. G. Miller and R. W. Kavanagh, *Nucl. Phys.* **A94**, 261 (1967).

<sup>6</sup>T. A. Belote, W. E. Dorenbusch, and J. Rapaport, *Nucl. Phys.* **A109**, 666 (1968).

<sup>7</sup>J. M. Laget and J. Gastebois, *Nucl. Phys.* **A122**, 431 (1968).

<sup>8</sup>C. Shin, B. Povh, K. Schadewaldt, and J. P. Wurm, *Phys. Rev. Letters* **22**, 1124 (1969).

<sup>9</sup>M. J. Schneider and W. W. Daehnick, *Phys. Rev. C* **4**, 1649 (1971).

<sup>10</sup>C. C. Lu, M. S. Zisman, and B. G. Harvey, *Phys. Rev.* **186**, 1086 (1969).

<sup>11</sup>G. Bruge and R. F. Leonard, *Phys. Rev. C* **2**, 2000 (1970).

<sup>12</sup>J. M. Bjerregaard, P. F. Dahl, O. Hansen, and G. Sidenuis, *Nucl. Phys.* **51**, 641 (1964).

<sup>13</sup>S. A. Hjorth, *Arkiv Fysik* **33**, 147 (1966).

<sup>14</sup>J. D. Anderson, C. Wong, and J. W. McClure, *Nucl. Phys.* **36**, 161 (1962).

<sup>15</sup>J. W. Nelson, H. S. Plendl, and P. H. Davis, *Phys. Rev.* **125**, 2005 (1962).

<sup>16</sup>F. D. Becchetti, Jr., D. Dehnard, and T. G. Dzubay, in *Proceedings of the Second Conference on Nuclear Isospin, Asilomar-Pacific Grove, California, 1969*, edited by J. D. Anderson, S. D. Bloom, J. Cerny, and W. W. True (Academic, New York, 1969), p. 171.

<sup>17</sup>P. G. Roos and C. D. Goodman, in *Proceedings of the Second Conference on Nuclear Isospin, Asilomar-Pacific Grove, California, 1969* (See Ref. 16), p. 297.

<sup>18</sup>G. Bruge, A. Chaumeaux, Ha Duc Long, P. Roussel, and L. Valentin, *Bull. Am. Phys. Soc.* **15**, 1208 (1969).

<sup>19</sup>T. G. Dzubay, R. Sherr, F. D. Becchetti, and D. Dehnard, *Nucl. Phys.* **A142**, 488 (1970).

<sup>20</sup>D. O. Wells, *Nucl. Phys.* **66**, 562 (1965).

<sup>21</sup>A preliminary account of this work was given by L. E. Samuelson, R. A. Warner, W. H. Kelly, R. R. Todd, and Wm. C. McHarris, *Bull. Am. Phys. Soc.* **16**, 12 (1971); and L. E. Samuelson, R. A. Warner, W. H. Kelly, and

F. M. Bernthal, *Bull. Am. Phys. Soc.* **17**, 584 (1972).

<sup>22</sup>R. DelVecchio, R. F. Gibson, and W. W. Daehnick, *Phys. Rev. C* **5**, 446 (1972).

<sup>23</sup>L. Wolfenstein, *Phys. Rev.* **82**, 690 (1951).

<sup>24</sup>W. Hauser and H. Feshbach, *Phys. Rev.* **87**, 366 (1952).

<sup>25</sup>L. C. Biedenharn and M. E. Rose, *Rev. Mod. Phys.* **25**, 729 (1953).

<sup>26</sup>G. R. Satchler, *Phys. Rev.* **94**, 1304 (1954); **104**, 1198 (1956); *Phys. Rev.* **111**, 1747(E) (1958).

<sup>27</sup>E. Sheldon and D. M. Van Patter, *Rev. Mod. Phys.* **38**, 143 (1966).

<sup>28</sup>J. B. McGrory, Oak Ridge National Laboratory, private communication.

<sup>29</sup>K. A. Kraus and F. Nelson, in *Proceedings of the International Conference on the Peaceful Uses of Atomic Energy, Geneva, 1955* (United Nations, New York, 1956), Vol. 7, p. 113.

<sup>30</sup>A. D. Horton, *ORNL Master Analytical Manual*, TID-7015, Sec. 1, April 1958, Nickel, Spectrophotometric Di Methyl Glyoxime - Bromine Oxidation Method, Method Nos. 1 215411 and 9 00715411 (11-9-56).

<sup>31</sup>POLYPHEMUS, a pulse-height analysis computer code written by R. Au, Michigan State University Cyclotron Laboratory (unpublished).

<sup>32</sup>J. T. Routti and S. G. Prussin, *Nucl. Instr. Methods* **72**, 125 (1969).

<sup>33</sup>R. C. Greenwood, R. G. Helmer, and R. J. Gehrke, *Nucl. Instr. Methods* **77**, 141 (1970).

<sup>34</sup>J. B. Marion, *Nucl. Data* **A4**, 301 (1968).

<sup>35</sup>C. M. Lederer, J. M. Hollander, and I. Perlman, *Table of Isotopes* (Wiley, New York, 1967), 6th ed.

<sup>36</sup>S. M. Brahmavar, J. H. Hamilton, A. V. Ramayya, E. F. Zganjar, and C. E. Bemis, Jr., *Nucl. Phys.* **A125**, 217 (1969).

<sup>37</sup>A. J. Haverfield, F. M. Bernthal, and J. M. Hollander, *Nucl. Phys.* **A94**, 337 (1967).

<sup>38</sup>D. C. Camp and G. L. Meredith, *Nucl. Phys.* **A166**, 349 (1971).

<sup>39</sup>EVENT, a computer code written by D. Bayer, Michigan State University Cyclotron Laboratory (unpublished).

<sup>40</sup>EVENT RECOVERY, a coincidence sorting computer code written by D. B. Beery and G. C. Giesler, Michigan State University Cyclotron Laboratory (unpublished).

<sup>41</sup>W. B. Ewbank and S. Raman, *Nucl. Data* **B3**(Nos. 3, 4), 187 (1970).

<sup>42</sup>P. Goode and L. Zamick, *Phys. Rev. Letters* **22**, 958 (1969).

<sup>43</sup>S. D. Bloom, L. G. Mann, and J. A. Miskel, *Phys. Rev.* **125**, 2021 (1962).

<sup>44</sup>H. Daniel, *Rev. Mod. Phys.* **40**, 659 (1968).

<sup>45</sup>R. K. Sheline and R. W. Stoughton, *Phys. Rev.* **87**, 1 (1952).

<sup>46</sup>H. Maria, J. Dalmaso, C. Ardisson, and C. Ythier,

- Compt. Rend. B271, 165 (1970).
- <sup>47</sup>C. Maples, G. W. Goth, and J. Cerny, Nucl. Data A2(Nos. 5, 6), 429 (1966).
- <sup>48</sup>B. H. Armitage, A. T. G. Ferguson, G. C. Neilson, and W. D. N. Pritchard, Nucl. Phys. A133, 241 (1969).
- <sup>49</sup>L. E. Samuelson, Ph.D. thesis, Michigan State University, 1972 (unpublished).
- <sup>50</sup>J. Vervier, Nucl. Phys. 78, 497 (1966).
- <sup>51</sup>H. J. Hausman, R. M. Humes, and R. G. Seyler, Phys. Rev. 164, 1407 (1967).
- <sup>52</sup>L. L. Lee, Jr., and J. P. Schiffer, Phys. Letters 4, 104 (1963).
- <sup>53</sup>J. R. Huizenga and A. A. Katsanos, Nucl. Phys. A98, 614 (1967).
- <sup>54</sup>E. Sheldon and P. Gantenbein, J. Appl. Math. Phys. (ZAMP) 18, 397 (1967); E. Sheldon and R. M. Strang, Comp. Phys. Commun. 1, 35 (1969).
- <sup>55</sup>E. H. Auerbach, ABACUS-II, Brookhaven National Laboratory Report No. BNL-6562 (to be published).
- <sup>56</sup>F. Perey, *Direct Interactions and Nuclear Reaction Mechanism* (Gordon and Breach, New York, 1963).
- <sup>57</sup>F. Perey and B. Buck, Nucl. Phys. 32, 353 (1962).
- <sup>58</sup>E. Sheldon, Rev. Mod. Phys. 35, 795 (1963).
- <sup>59</sup>K. M. Thompson and C. R. Gruhn, Nucl. Instr. Methods 74, 309 (1969).
- <sup>60</sup>GADFIT, computer code written by R. A. Warner, Michigan State University Cyclotron Laboratory (unpublished).
- <sup>61</sup>The absolute intensity standards were obtained from the Radiation Materials Corporation of Waltham, Massachusetts.
- <sup>62</sup>P. A. Moldauer, Phys. Rev. 123, 968 (1961); 135, B642 (1964); Rev. Mod. Phys. 36, 1079 (1964).
- <sup>63</sup>R. V. Jones, W. Dobrowolski, and C. D. Jeffries, Phys. Rev. 102, 738 (1956).
- <sup>64</sup>R. L. Auble, Wm. C. McHarris, and W. H. Kelly, Nucl. Phys. A91, 225 (1967), and references cited therein.
- <sup>65</sup>W. Menti, Helv. Phys. Acta 40, 981 (1967).
- <sup>66</sup>S. S. Hanna, J. Heberle, C. Littlejohn, G. J. Perlow, R. S. Preston, and D. H. Vincent, Phys. Rev. Letters 4, 177 (1960).
- <sup>67</sup>M. N. Rao, Nucl. Data B3(Nos. 3,4), 43 (1970).
- <sup>68</sup>M. R. Najam, W. F. Davidson, W. M. Zuk, L. E. Carlson, and M. A. Awal, Nucl. Phys. A173, 577 (1971).
- <sup>69</sup>E. C. Halbert, J. B. McGrory, B. H. Wildenthal, and S. P. Pandya, in *Advances in Nuclear Physics*, edited by M. Baranger and E. Vogt (Plenum Press, New York, 1971), Vol. 4.
- <sup>70</sup>S. A. Moszkowski, in *Alpha-, Beta-, and Gamma-Ray Spectroscopy*, edited by K. Siegbahn (North-Holland, Amsterdam, 1965), Vol. 2, Chap. XV.

## New Aluminum Isotope; Mass and $\beta$ Decay of the $T_z = \frac{5}{2}$ Nuclide $^{31}\text{Al}$ and the Mass of $^{34}\text{P}^\dagger$

David R. Goosman and David E. Alburger

Brookhaven National Laboratory, Upton, New York 11973

(Received 2 February 1973)

The first reported measurements of the  $\beta$  decay, half-life, and mass of  $^{31}\text{Al}$  are presented. The new activity was produced by the  $^{18}\text{O}(^{18}\text{O}, \alpha p)^{31}\text{Al}$  reaction using 41-MeV incident  $^{18}\text{O}$  ions, and was transferred pneumatically to a remotely located station where delayed  $\gamma$  rays and  $\beta$  rays were counted with Ge(Li) and NE 102 detectors, respectively.  $\gamma$ -ray energies (in keV) and relative intensities for the  $^{31}\text{Si}$  daughter transitions are  $621.81 \pm 0.30$  (9.94  $\pm$  0.65),  $752.23 \pm 0.30$  (18.5  $\pm$  0.8),  $1564.49 \pm 0.30$  (17.3  $\pm$  1.6),  $1694.73 \pm 0.30$  (58.9  $\pm$  1.6), and  $2316.64 \pm 0.40$  (72.8  $\pm$  1.8). The  $^{31}\text{Si}$  excitation energies (in keV) and relative  $\beta$  branching intensities are  $752.24 \pm 0.30$  (<3.0),  $1694.78 \pm 0.30$  (49.0  $\pm$  1.7), and  $2316.73 \pm 0.40$  (100  $\pm$  2.5). A tentative  $\beta$ -ray transition to a state at  $E_x = 2787.7 \pm 0.8$  keV is also observed. Upper limits on the strength of some possible  $\gamma$ -ray transitions following  $\beta$  decay to higher levels are given.  $^{31}\text{Al}$  decays with a half-life of  $644 \pm 25$  msec. By measuring the energy spectra of  $\beta$  rays populating the second and third excited states of  $^{31}\text{Si}$  the mass excess of  $^{31}\text{Al}$  has been measured to be  $-15008 \pm 100$  keV. The mass excess of  $^{34}\text{P}$  has been remeasured by a similar technique to be  $-24550 \pm 90$  keV, and this value has been used to revise previous predictions for the masses of  $^{33}\text{Si}$  and  $^{35}\text{P}$ . The masses of several  $T_z = \frac{5}{2}$  and  $T_z = 3$  nuclides in the  $2s-1d$  shell are compared with theoretical estimates. The  $\beta$ -decay measurements for  $^{31}\text{Al}$  are shown to be in poor agreement with simple collective-model calculations, and in good agreement with recent detailed shell-model calculations.

### I. INTRODUCTION

The study of light nuclei with large neutron excess is important for several reasons. Mass measurements of these nuclei provide tests for various extrapolation procedures used to estimate

masses. The boundaries of the region of particle stability for neutron-rich nuclei as predicted by Garvey *et al.*<sup>1</sup> are surprisingly far from the valley of stability. The calculated location of these boundaries depends presently upon the measured masses of nuclei relatively close to  $\beta$  stability.